

QUATERNARY GEOLOGY OF THE UTAH FORGE SITE AND VICINITY, MILLARD AND BEAVER COUNTIES, UTAH

by Tyler Knudsen, Emily Kleber, Adam Hiscock, and Stefan M. Kirby

Utah Geological Survey, Salt Lake City, Utah



Miscellaneous Publication 169-B

Utah Geological Survey

a division of

UTAH DEPARTMENT OF NATURAL RESOURCES

This paper is part of *Geothermal Characteristics of the Roosevelt Hot Springs System and Adjacent FORGE EGS Site, Milford, Utah*. <https://doi.org/10.34191/MP-169>

Bibliographic citation:

Knudsen, T., Kleber, E., Hiscock, A., and Kirby, S.M., 2019, Quaternary geology of the Utah FORGE site and vicinity, Millard and Beaver Counties, Utah, *in* Allis, R., and Moore, J.N., editors, *Geothermal characteristics of the Roosevelt Hot Springs system and adjacent FORGE EGS site, Milford, Utah: Utah Geological Survey Miscellaneous Publication 169-B*, 21 p., 2 appendices, <https://doi.org/10.34191/MP-169-B>.

QUATERNARY GEOLOGY OF THE UTAH FORGE SITE AND VICINITY, MILLARD AND BEAVER COUNTIES, UTAH

by Tyler Knudsen, Emily Kleber, Adam Hiscock, and Stefan M. Kirby

ABSTRACT

We present new Quaternary geologic mapping, geomorphic analysis, and luminescence geochronology to better understand the Quaternary geologic history of the Utah FORGE site near Milford, Utah. Late Cenozoic unconsolidated deposits in the map area are predominantly coarse-grained alluvial-fan deposits sourced from the Mineral Mountains. Boulder-rich basin-fill deposits are the oldest mapped unconsolidated unit (Taf) representing debris shed from the rapidly rising ancestral Mineral Mountains during Miocene to Pliocene time. Erosion of the Mineral Mountains continued into the early Pleistocene, forming the deeply embayed canyons and generally mature topography of the range today. In early middle Pleistocene time (~0.7–0.5 Ma), rhyolitic lava flows and domes partially filled pre-existing canyons. By the late middle Pleistocene (~0.5–0.1 Ma), alluvial fans began aggrading east, deep into the canyons and abutting against the rhyolitic flows. The distal ends of the alluvial fans were extensively reworked and etched by shorelines of Lake Bonneville, which occupied Milford Valley from about 20 to 18 ka. The recession of Lake Bonneville about 18 ka and resultant lowering of base level may have spurred the deep incision of Negro Mag Wash (NMW), Ranch Canyon, and Corral Canyon that has rendered older alluvial fans inactive.

We mapped three fault zones near the Utah FORGE site that had apparent Quaternary displacement: the Negro Mag fault (NMF), the Opal Mound fault (OMF), and the Mineral Mountains West fault zone (MMWFZ). The steeply dipping NMF trends east-west across much of the Mineral Mountains and bounds the northern margin of the Roosevelt Hot Springs geothermal area. We found no definitive evidence for displacement of Quaternary deposits along the inferred trace of the NMF and suspect the fault may be pre-Quaternary in age.

The steeply east-dipping, north-trending OMF defines the western boundary of the Roosevelt Hot Springs geothermal system. The fault displaces late Pleistocene alluvial-fan deposits as much as 18 m. Hot springs emanating from the fault zone have deposited abundant siliceous sinter along the fault. Sinter deposition and faulting have been contemporaneous as evidenced by buried horizons of sinter detected in well logs, and by possible fault-rotated blocks of sinter mapped in the fault zone. However, Holocene sinter as young as 1.6 to 1.9 kyr covers the southern end of the fault and appears unbroken. Development of the OMF scarp has been greatly influenced by differential erosion of siliceous sinter exposed along the fault. Latest movement on the OMF was in the late Pleistocene (12–126 kyr), but its resultant scarp appears older than scarps formed by the nearby Lake Bonneville shoreline (>18 ka) and scarps formed by the MMWFZ.

The north-south-trending MMWFZ extends for about 40 km from near the Utah FORGE site to south of Minersville. The fault zone has produced a series of east- and west-dipping scarps on late Pleistocene alluvial fans that are less than 5 m high. South of Corral Canyon, multiple strands of the fault zone converge into a single fault that has produced a scarp as high as about 12 m. MMWFZ scarps are deeply dissected and display similar scarp morphologies as the nearby Bonneville shoreline that formed about 18 ka. Unfaulted latest Pleistocene to Holocene alluvium covers parts of the fault zone, indicating that the most recent movement on the fault zone is late Pleistocene.

INTRODUCTION

The Utah FORGE site is in the eastern Basin and Range Province (Figure 1), a region of east-west extension that covers much of the southwestern United States. The province consists of north-south-striking, range-bounding normal faults that define a series of bedrock horst blocks and corresponding basins. Basin and Range extension began in the early Miocene (ca. 17.5 Ma) and continues today (Dickinson, 2006). Within the Basin and Range, most developed geothermal systems are fault controlled (Faulds and others, 2011). In the Sevier Desert of southwestern Utah, several geothermal systems may have magmatic sources (Faulds and others, 2011), and deep-seated faults allow for hydrothermal circulation. Some late Quaternary normal faulting in the Sevier Desert about 75 km north of the FORGE site may be related to rift-assisted magmatism (Stahl and Niemi, 2017; Figure 1).

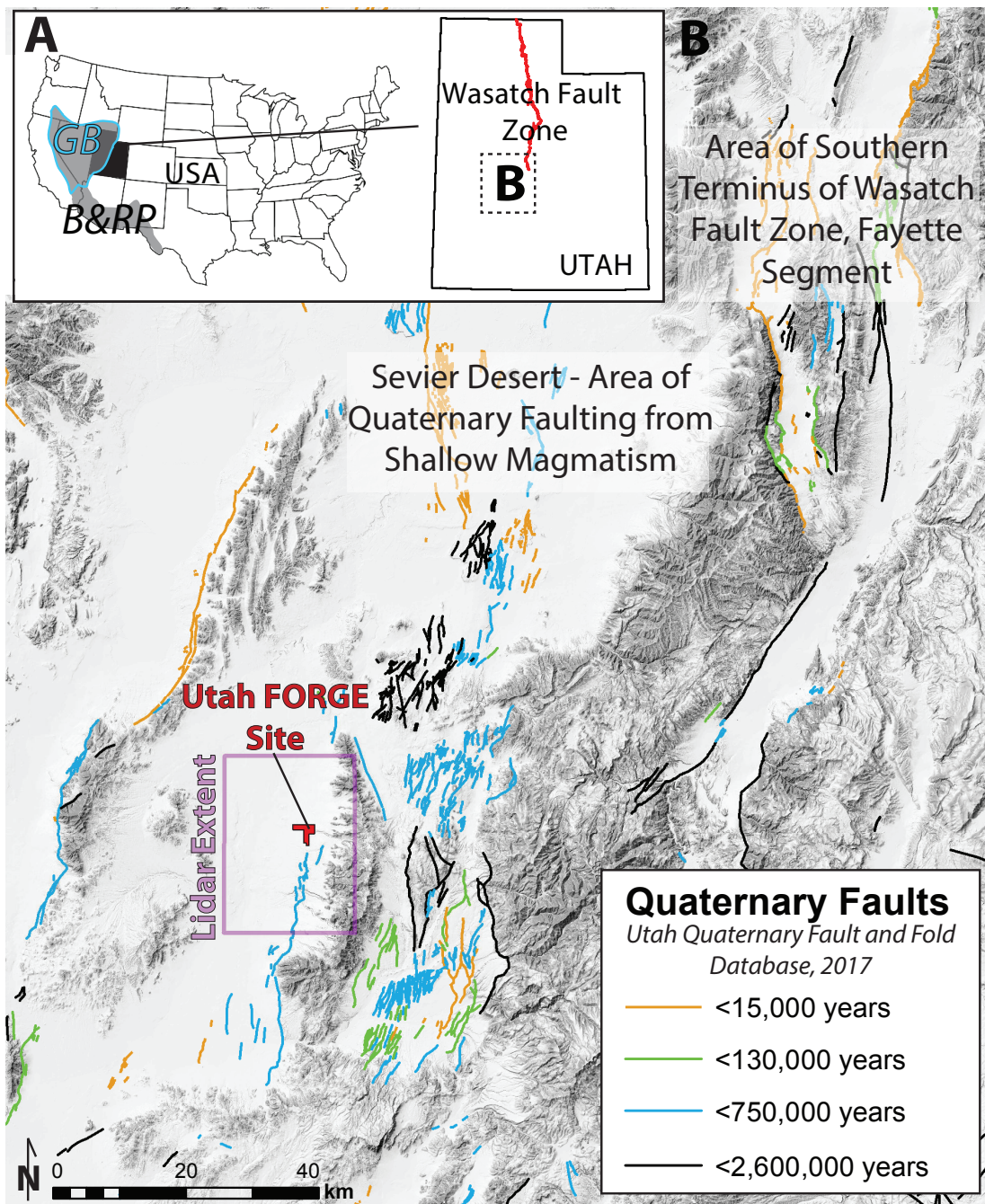


Figure 1. (A) Regional overview of the study area relative to the Great Basin (GB), Basin and Range Province (B&RP), and the Wasatch fault zone (WFZ) in Utah. (B) Regional Quaternary faults near the Utah FORGE site include the southern terminus of the WFZ and faulting that may be driven by shallow magmatism in the Sevier Desert (Stahl and Niemi, 2017); colored fault lines indicate age of the most recent surface-rupturing movement.

The Utah FORGE site is on the western flank of the Mineral Mountains, a 45-km-long, north-south-trending mountain range consisting primarily of late Oligocene to late Miocene intrusive rocks (Nielsen and others, 1986; Kirby, 2019). Late Cenozoic unconsolidated deposits in the map area consist of coarse-grained alluvial deposits of late Tertiary to Holocene age, and coarse- and fine-grained lacustrine sediment deposited during at least two Quaternary lake cycles. The FORGE site is 2 km west of the Roosevelt Hot Springs (RHS) hydrothermal system that currently generates up to 35 MWe of gross power at the Blundell Power Plant (Simmons and others, 2016) (Figure 2). Quaternary hot spring deposits are common along the western margin of the RHS geothermal area. Thin eolian sand deposits are present throughout the study area, and form dunes and partially stabilized sand sheets and sand mounds. Late Tertiary and Quaternary rhyolitic lava flows and domes are present in the central Mineral Mountains. Three fault zones within the study area having suspected Quaternary movement are the north-south-trending Mineral Mountains West fault zone (MMWFZ), the Opal Mound fault (OMF), and the east-west-trending Negro Mag fault (NMF; Figure 2).

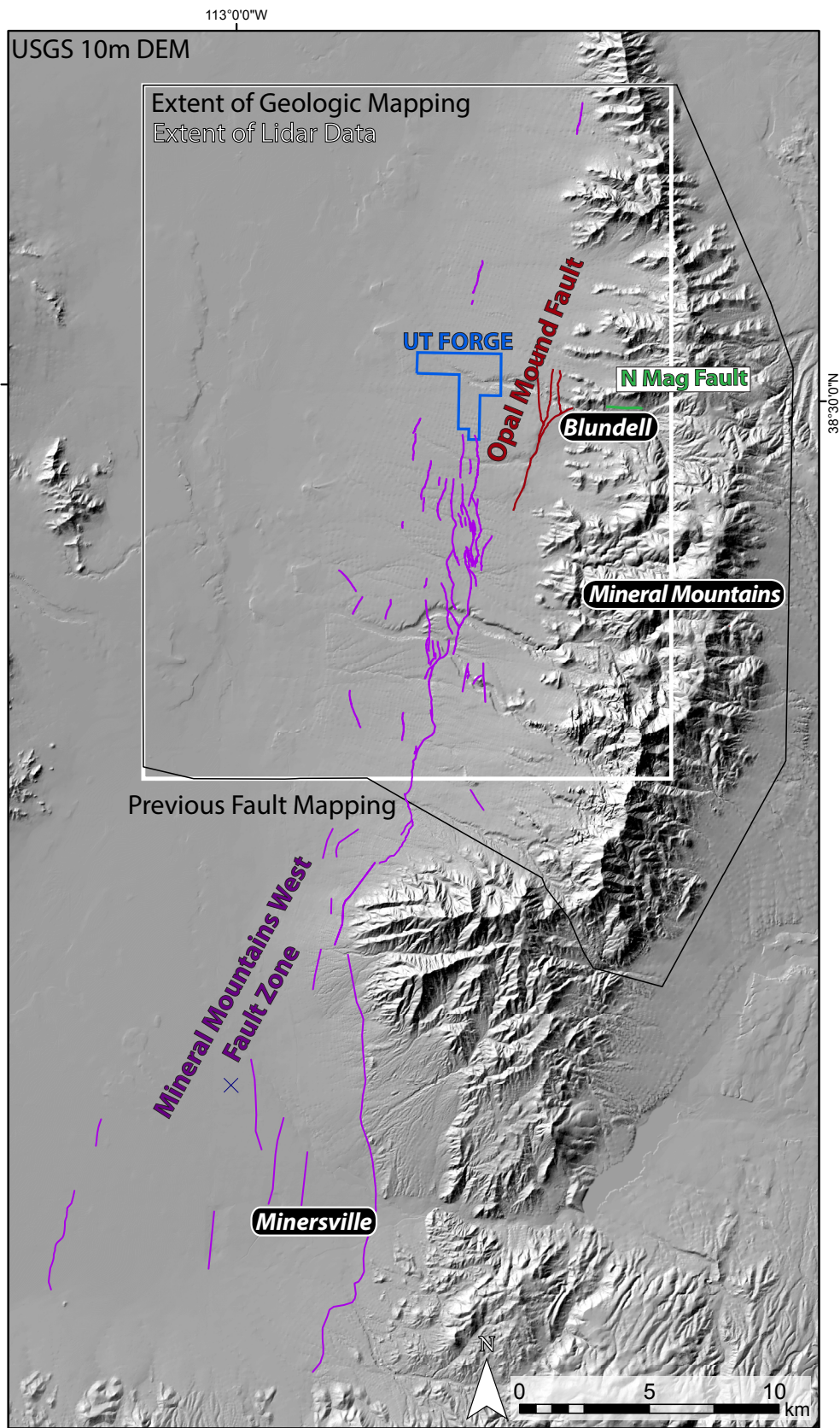


Figure 2. Extent of Quaternary geologic mapping based on available lidar elevation data and the extent of the combined bedrock Quaternary geologic map presented in Kirby (2019). The surface traces of the OMF and the MMWFZ are also shown. The location of the MMWFZ south of the lidar-mapping area is depicted at a reconnaissance level based on previously published mapping (Rowley and others, 2005; Utah Geological Survey, 2017), satellite data, and aerial photographs.

Petersen (1975) produced one of the earliest geologic maps of the RHS geothermal area that focused on Quaternary unconsolidated deposits and faulting. Anderson and Bucknam (1979) investigated fault scarps along the eastern margin of Milford Valley as part of a larger study of Quaternary fault scarps in the Richfield 1° x 2° quadrangle. Brogan and Birkhahn (1981) completed detailed surficial mapping, topographic profiling, and paleoseismic trench investigations along Quaternary faults near the RHS geothermal area. Geologic mapping by Hintze and others (2003; 1:62,500 scale) and Rowley and others (2005; 1:100,000 scale) subdivided unconsolidated units in the Richfield and Beaver 30' x 60' quadrangles, respectively, that collectively cover the Mineral Mountains and eastern Milford Valley.

Our mapping provides new information on the distribution and relative age of Quaternary unconsolidated deposits near the Utah FORGE site. This mapping also greatly improves information on the location, extent, and relative age of Quaternary-active fault traces. These data may be used to update geologic models and to provide updated information for seismic-hazard analyses.

METHODS

Geologic Mapping

We mapped late Cenozoic surficial deposits and Quaternary fault traces in an area encompassing 850 km² centered on the Utah FORGE site and the adjacent RHS geothermal area. The map encompasses an area that extends from Milford in the southwest corner to nearly the northern end of the Mineral Mountains in the northeast corner (Figure 2). Geologic mapping was based primarily on the interpretation of a digital elevation model (DEM) derived from 0.5-m airborne lidar (light detection and ranging) data acquired in the fall of 2016. Black-and-white and color aerial photography having various dates and scales (1953 AMS, 1:63,300 scale; 1955 GS-VJI, 1:37,400 scale; 1979 CSR-F, 1:25,000 scale) was also reviewed. We discovered that many prominent lineaments and tonal changes on the photos—some of which were mapped as fault scarps by some previous mappers—are the result of extensive range-management and fire-suppression/mitigation efforts in the area that have spanned several decades. Mapping was performed at 1:10,000 scale, but for convenience, is here combined with recently mapped bedrock geology at 1:24,000 scale (Kirby, 2019, Plates 1 and 2). We performed field mapping intermittently from August to December of 2017. We distinguished the relative age of alluvial-fan deposits based on surface morphology and degree of pedogenic carbonate development.

Geochronology

Infrared Stimulated Luminescence (IRSL) is a technique that uses infrared light to release trapped electrons within a crystal lattice to calculate an age. The infrared luminescence signal from potassium feldspar sand grains yields an estimate for the last time the grains were exposed to sunlight and thus infer a burial age (Rittenour, 2008; Rhodes, 2011). Before deposition, the grains are “bleached” by exposure to the sun. The bleaching process removes any trapped electron charge by brief natural light exposure during the transport of grains on the surface. The sand grains are deposited, buried, and then begin the process of being exposed to ionizing radiation from the surrounding soil. Over time, the ionizing radiation creates a charge by energizing electrons and moving them out of their normal orbits and into the crystal lattice of the potassium feldspar crystal. IRSL stimulates aliquots (i.e., samples) of sand grains that have not been exposed to light since burial using intense infrared light (880 ± 80 nm). These aliquots then luminesce from electrons being released from the crystal lattice. The luminescence decays until there is no more signal. From measuring the amount of luminescence from the sand grain, the equivalent dose (D_E), or amount of radiation energy the crystal has been exposed to since burial, is calculated. Another measurement of the ionizing radiation in the surrounding soil is taken to calculate the amount of radiation the sample has been exposed to over time (i.e., dose rate). The burial age of the deposit is calculated by dividing the D_E by the dose rate of the deposit sampled.

In August 2017 we excavated five test pits into various alluvial-fan deposits to better understand the composition and age of the sediments. In addition to detailed descriptions of sediment composition, texture, and soil development, we collected and submitted eight samples for IRSL dating at the Utah State University Luminescence Laboratory (<https://www.usu.edu/geo/luminlab/>). Based on geologic mapping, the burial ages of feldspar sand on the footwall of normal fault scarps will give maximum ages for fan-surface abandonment by vertical fault offset. We collected samples in light-safe tubes of sand-size grains in buried sheet flow deposits within mapped alluvial-fan units. Special care was taken when sampling to avoid poorly sorted deposits where sand grains may have not been completely bleached during deposition. Quartz and feldspar grains from 63 to 250 µm were separated and analyzed at the Utah State University Luminescence Lab. IRSL sample locations are shown on Figure 3 and final IRSL results are in Table 1. Soil logs with IRSL ages are in Appendix 1.

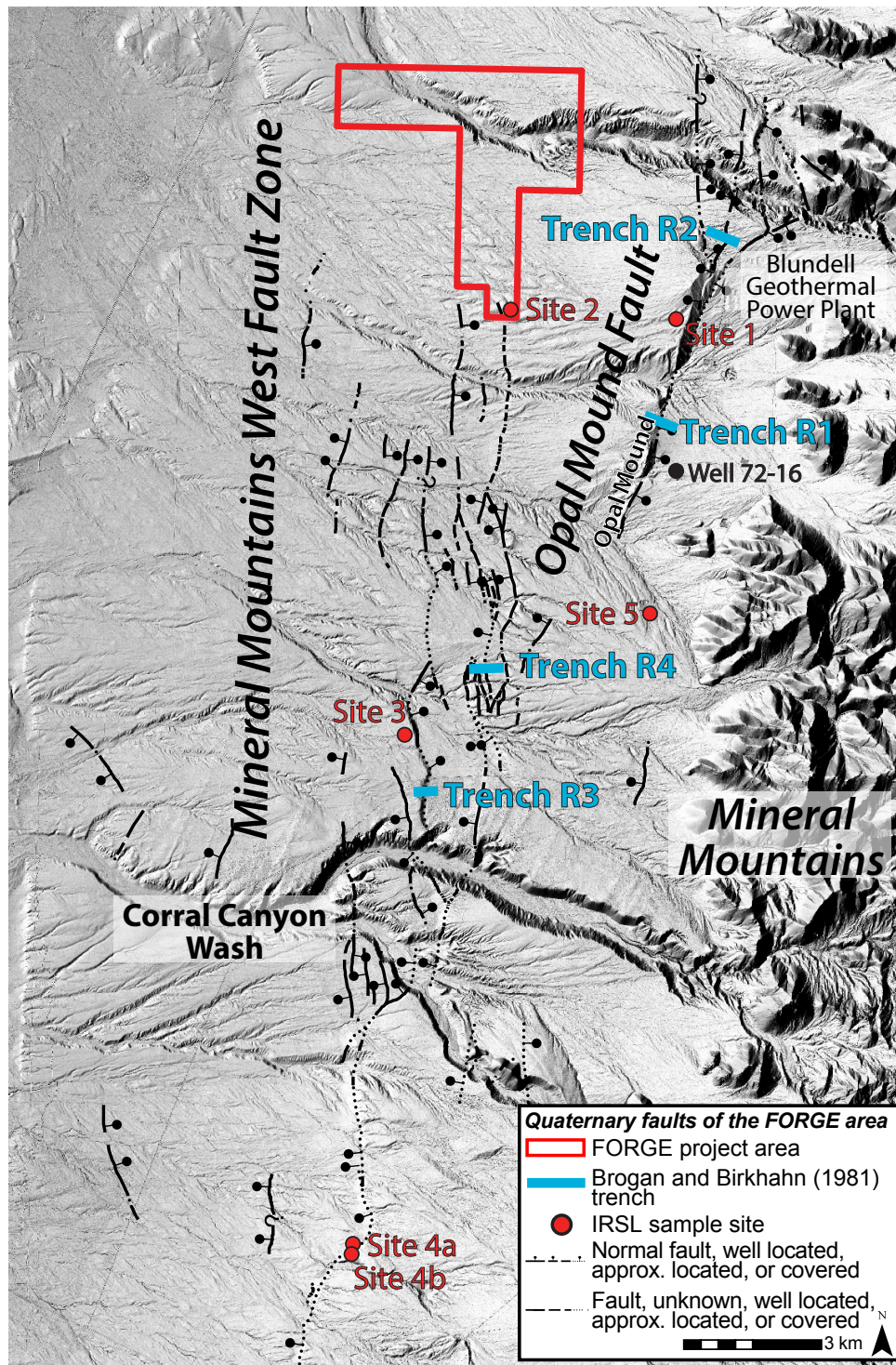


Figure 3. Half-meter slope-shade image derived from lidar of the fault systems around the RHS. The east-dipping OMF is considered a hydrologic barrier to geothermal fluid flow. The northern extent of the MMWFZ is a graben system that initiates 8 km south of the FORGE project area. The graben has internal horsts and grabens, with some discontinuous faults outside of the surface expression of the main graben.

Geomorphic Analysis

We used slope and aspect maps, hillshade models, and elevation contours derived from the 0.5-m lidar DEM to describe fault-scarp morphologies. To compare fault scarps along strike, we generated elevation profiles from the DEM using Global Mapper v.14. Using a slope map, we collected elevation profiles perpendicular to fault scarps. Elevation profiles were sufficiently long to ensure complete capture of undeformed alluvial-fan surfaces on the hanging wall and footwall of the faults (Figure 4).

Table 1. Final IRSL age information results received January 31, 2018 from the Utah State University Luminescence lab.

Sample num.	USU num.	Num. of aliquots ¹	Dose rate (Gy/ka)	$D_E^2 \pm 2\sigma$ (Gy)	Fading Rate ³ $\pm 1\sigma$ g_{2days} (%/decade)	IRSL age $\pm 2\sigma$ (ka)
FORGE 1 – OSL2	USU-2680	19 (19)	7.43 \pm 1.24	255.85 \pm 21.81	4.8 \pm 0.9	55.55 \pm 12.07
FORGE 2 – OSL3	USU-2681	14 (16)	9.13 \pm 1.67	272.54 \pm 25.13	8.9 \pm 2.4	80.12 \pm 22.60
FORGE 5 – OSL1	USU-2682	15 (16)	10.45 \pm 2.09	161.43 \pm 24.00	6.8 \pm 1.7	30.67 \pm 9.25
FORGE 3 – OSL7	USU-2683	20 (23)	11.29 \pm 2.25	153.87 \pm 27.94	9.8 \pm 2.1	41.41 \pm 12.89
FORGE 4a – OSL4	USU-2684	17 (17)	5.99 \pm 0.77	45.76 \pm 4.78	11.7 \pm 2.74	25.26 \pm 6.40
FORGE 4a – OSL5	USU-2685	17 (17)	6.34 \pm 0.92	42.71 \pm 3.21	10.8 \pm 1.74	21.53 \pm 4.31
FORGE 4a – OSL8	USU-2686	12 (12)	6.58 \pm 0.85	39.34 \pm 2.87	10.7 \pm 1.94	14.95 \pm 4.33
FORGE 4b – OSL6	USU-2687	13 (13)	8.22 \pm 2.36	58.12 \pm 5.77	6.9 \pm 1.4	>14.48 \pm 5.43

¹ Age analysis using the IRSL (50°C) and elevated temperature (225°C) pIR IRSL protocol of Buylaert et al. (2009). Number of aliquots used in age calculation and number of aliquots analyzed in parentheses.

² Equivalent dose (DE) and IRSL age calculated using the Central Age Model (CAM) of Galbraith and Roberts (2012).

³ IRSL age on each aliquot corrected for fading following the method by Auclair et al. (2003) and correction model of Huntley and Lamothe (2001).

⁴ Average fading rate from all site 4a samples (9.9 \pm 1.3%/decade) is likely underestimating true fading rate values, maximum fading rate for Huntley and Lamothe (2001) model of 10.0 \pm 1.0%/decade applied to all aliquots for fading-corrected IRSL ages.

We used Scarp Offset (v. 4g) (DuRoss, in preparation) in MatLab (v. R2017a) to analyze the fault-scarp profiles for the MMWFZ and OMF within the airborne lidar coverage area (Figure 4). This script uses a graphical user interface (GUI) that displays elevation versus distance and slope versus distance to allow the user to select the upper and lower bounds (i.e., fault offset surfaces) and the fault-scarp slope. The GUI plots and displays elevation vs. distance as well as slope vs. distance. Once the upper and lower bounds of the scarp are defined by the user, the script produces multiple measurements of the scarp to determine a preferred mean, or midpoint offset, value for the scarp and a minimum-maximum range. For each elevation profile, we made three measurements of the upper and lower bounds of the fault scarp based on (1) slope change in the topographic profile, (2) slope changes in the slope vs. distance plot, and (3) all profile data on the hanging-wall and footwall surfaces, except for the scarp (Appendix 2). The value used in each scarp height and scarp slope measurement is the mean value of these three measurements. These measurements were combined along strike to show the distribution of first-order measurements of scarp morphology of the OMF and MMWFZ (Figure 4).

LATE NEOGENE–QUATERNARY STRATIGRAPHY

Pre-Quaternary Volcanic Rocks and Alluvium

The oldest unconsolidated deposits exposed in the map area are Tertiary basin-fill deposits (map unit Taf) that crop out in two small areas: one area is north of Opal Mound and the other area is along the northern rim of Corral Canyon (see Kirby, 2019, Plate 1). North of Opal Mound, the east-dipping OMF has exhumed Taf deposits that are well exposed in a roadcut (Figure 5). Taf deposits consist of coarse, poorly sorted, non-stratified debris with boulders as large as 5 m in greatest dimension. Clasts are predominantly Precambrian banded gneiss and granitic intrusive rocks sourced from the Mineral Mountains. The abundance of large boulders of Precambrian metamorphic rocks on Taf slopes north of Opal Mound led Petersen (1975) to map much of the outcrop as Precambrian bedrock. Taf material was likely deposited on alluvial fans as debris flows and debris floods, although no original fan morphology remains. Boulder-rich Taf deposits are strikingly different than adjacent gruss-dominated, middle-fan alluvial units (Qaf₂ and Qaf₃) that were deposited in a comparatively low-energy environment. Obsidian, derived from ~0.8 to 0.5 Ma rhyolite flows (Lipman and others, 1978) in the Mineral Mountains, is common in all mapped Quaternary fan deposits except Taf, indicating that Taf predates the early to middle Pleistocene rhyolite eruptions. At Corral Canyon, Taf sediment is clearly overlain by a 7.9 Ma quartz-latite flow (Lipman and others, 1978; Sibbett and Nielson, 1980; Kirby, 2019, map unit MI on Plates 1 and 2). Therefore, the age of Taf is loosely constrained between about 0.8 Ma to older than 8 Ma. However, because the transport of very coarse Taf sediment could not have occurred in the modern, low-relief landscape that characterizes the area today, we suggest that deposition occurred in late Tertiary time when the Mineral Mountains were substantially more prominent. Rapid uplift of the Mineral Mountains began about 11–8 Ma (Evans and Nielson, 1982; Coleman and others, 2001) and the range acquired most of its relief by the end of the Pliocene (Machette, 1985). We interpret that Taf deposits represent coarse debris shed from the ancestral Mineral Mountains that was deposited on the margin of the developing Milford Valley in late Miocene to Pliocene time.

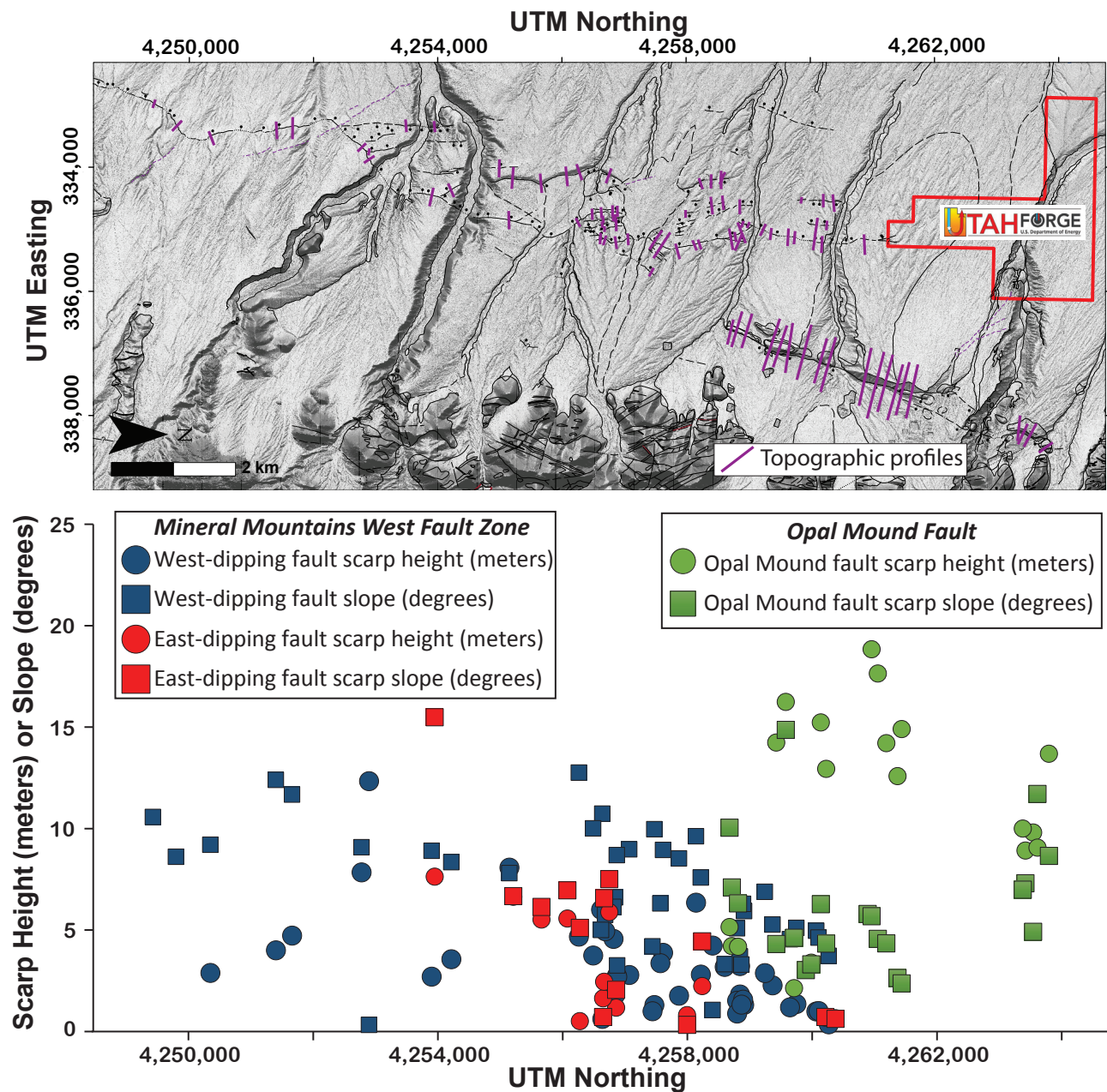


Figure 4. Lidar-derived slope-shade image of the western Mineral Mountains showing location and extent of fault-scarp elevation profiles. Graph shows fault scarp height and slope along strike of the MMWFZ and the OMF.

Quaternary Volcanic Rocks

Rhyolitic domes, lava flows, and air-fall and ash-flow tuffs were deposited from about 0.5 to 0.8 Ma (Lipman and others, 1978) on eroded bedrock surfaces and in canyons cut into the central Mineral Mountains (Rowley and others, 2005). The paleotopography preserved beneath the rhyolitic flows appears to be unchanged from the modern topography (Lipman and other, 1978). This indicates that the deeply embayed, low-gradient, and generally mature topography that characterizes the western flank of the central Mineral Mountains was likely established during the early Pleistocene, shortly after the range reached its maximum relief in the late Pliocene (Machette, 1985). The rhyolite flows in NM Wash (NMW; Bailey Ridge flow) and Wildhorse Canyon are well known for containing abundant implement-grade obsidian (Lipman and others, 1978). The distribution of obsidian clasts derived from the rhyolite helps constrain the relative ages of deposits that contain the clasts.



Figure 5. Coarse debris-flow deposits exposed in a road cut north of Opal Mound that are part of map unit Taf. The road cut is about 4 m high; photo taken September 7, 2017.

Quaternary Alluvial Deposits

Alluvial-fan deposits blanket much of the area near the Utah FORGE site (Kirby, 2019, Plate 1). The alluvium consists principally of pea-size gruss with minor cobbles and boulders derived from granitic intrusive and metamorphic rocks of the Mineral Mountains. Many fan surfaces are largely inactive and are incised by modern drainages. These older, dissected fan deposits are mapped as Qaf₃ and Qaf₂, where the subscript indicates relative age—Qaf₂ is younger and Qaf₃ is older. Older fan deposits typically extend from the valley interior upslope (at a remarkably consistent and relatively gentle 3° to 6° slope) into embayments cut deep into the Mineral Mountains. Modern drainages incise Qaf₂ alluvium as much as 9 m. Qaf₃ fan surfaces are incised as much as 45 m at NMW (Figure 6), and as much as 60 m at Ranch Canyon. Qaf₃ alluvium laps against the toe of the ~0.8-Ma Bailey Ridge flow, indicating that Qaf₃ is younger than ~0.8 Ma. Additionally, obsidian derived from the Bailey Ridge and Wildhorse Canyon flows is commonly intercalated with Qaf₃ and younger alluvial-fan deposits. The distal ends of Qaf₃ and Qaf₂ fans have been reworked by late Pleistocene Lake Bonneville and are deeply etched by the Bonneville highstand shoreline formed about 18 ka (Oviatt, 2015). Therefore, the age of Qaf_{2,3} alluvium is broadly constrained between about 0.8 Ma and 18 ka. However, based on weakly to moderately developed pedogenic carbonate observed in test pits excavated in older alluvial-fan deposits, we consider the sediment to be mostly late Pleistocene in age (~126–18 ka). IRSL burial ages for sediment collected from Qaf_{2,3} fans mostly support this conclusion. We obtained burial ages of 80.12 ± 22.60 ka, 55.55 ± 12.07 ka, and 41.41 ± 12.89 ka for samples collected from mapped Qaf₃ fan deposits (Figure 3 and Table 1). A single sample from a Qaf₂ fan yielded a 30.67 ± 9.25 ka burial age. A sample collected from a Qaf₂ fan surface at site 4b in the southern part of the map area yielded an anomalously young IRSL age of 14.48 ± 5.43 ka (Figure 3). The Qaf₂ fan surface having the anomalously young age is incised as much as 6 m and is surrounded by younger alluvium (Qaf_y and Qaf₁) (Figure 7). Less than 700 m east of site 4b, young, active-fan deposition (Qaf_y) is occurring at a higher elevation and is advancing downslope toward site 4b, burying the Qaf₂ surface. The fan surface at site 4b was possibly inundated by the distal end of some larger floods that discharged onto the active fan to the east.

Deep entrenchment of NMW, Ranch Canyon, and Corral Canyon of underlying alluvium has largely rendered older fan surfaces (Qaf₂ and Qaf₃) in the map area inactive. The excavation and down-gradient redistribution of alluvium driven by this period of incision resulted in the deposition of young fan alluvium (Qaf₁) at the mouths of the entrenched drainages. Young alluvial-fan deposits (Qaf₁) lack Bonneville shoreline etchings and clearly bury the Bonneville highstand shoreline and therefore are latest Pleistocene to Holocene in age. At about the same latitude of the entrenched drainages discussed above, the Beaver River is



Figure 6. View to the west into NMW near RHS. The wash is incised about 45 m into older alluvial-fan deposits (Qaf_3); photo taken September 18, 2017.

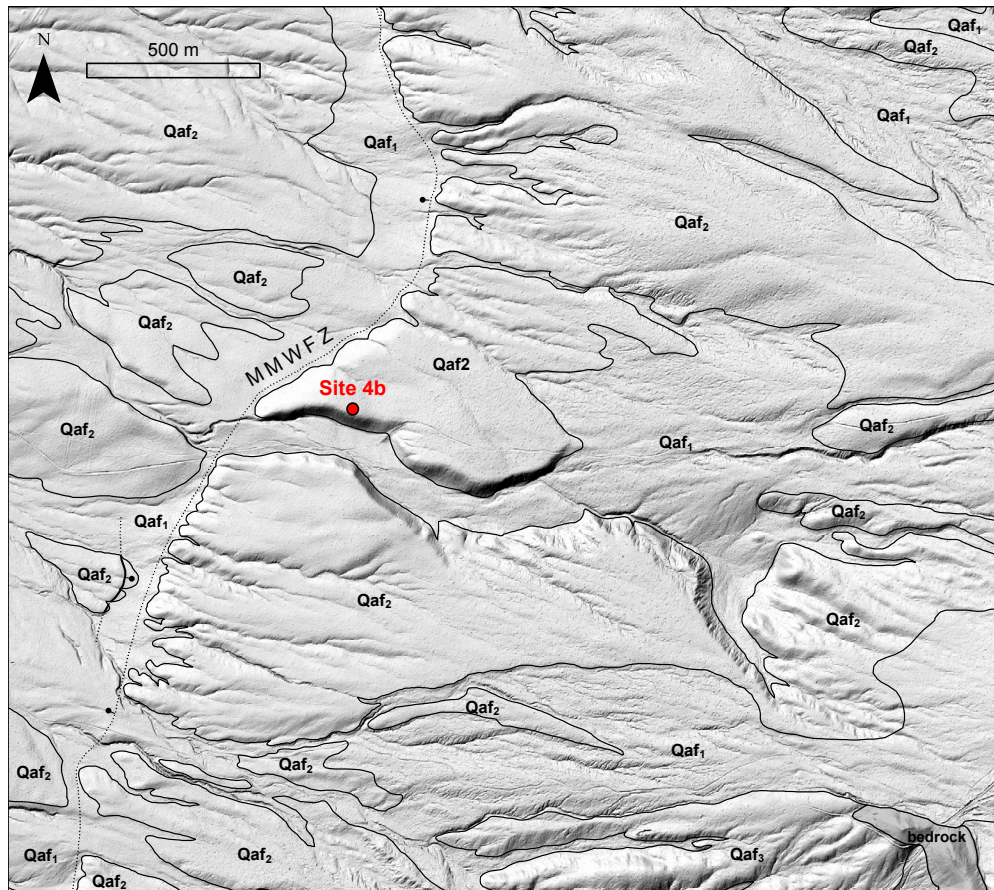


Figure 7. Lidar-derived hillshade image of MMWFZ scarp and Quaternary surficial units near IRSL sample site 4b. Bar and ball on downthrown side of fault; Qaf_1 =latest Pleistocene to Holocene alluvial-fan deposits; Qaf_2 , Qaf_3 =older late Pleistocene alluvial-fan deposits; Qaf_y =undivided Qaf_1 and Qaf_2 alluvial-fan deposits.

similarly incised into underlying lacustrine deposits as much as 18 m. This period of incision could be the result of local uplift, as proposed by Mower and Cordova (1974). Or, perhaps more likely, the incision is the result of the lowering of base level following the regression of Lake Bonneville from Milford Valley at about 18 ka (Hintze and Davis, 2003; Oviatt, 2015) (see Lacustrine Deposits section below). Since the intermittent streams that now occupy the entrenched washes are conspicuously underfit, the channels were probably cut by more substantial streams that flowed during a wetter and cooler climate. The wetter and cooler climate that contributed to the Bonneville lake cycle continued for approximately 3000 years following the regression of Lake Bonneville (Hintze and Davis, 2003; Oviatt, 2015). Therefore, deep incision of the fans may have largely occurred in latest Pleistocene to early Holocene time.

Additional younger, mostly Holocene fan alluvium (Qaf₁) fills small grabens and other low areas formed along the OMF and MMWFZ. The alluvial deposits locally bury strands of the fault zones and are not displaced by the faults.

Hot Spring Deposits

Hot spring deposits are common along the OMF where it defines the western boundary of the RHS geothermal area. We subdivided hot spring deposits into two units: siliceous-sinter-cemented alluvium (map unit Qafs) and primary, banded opaline sinter (Qs) (Kirby, 2019, Plates 1 and 2). Siliceous sinter was deposited by hot spring water emanating from vents along and closely parallel to the OMF. Unit Qafs consists principally of silica-cemented, pea-size gruss that resembles adjacent uncemented fan alluvium. Locally, the cement also contains calcium carbonate. Qafs tends to preserve geomorphic surfaces, such as fan surfaces and fault scarps, as they appeared at the time of spring activity and cementation. For example, stratified, sinter-cemented alluvium (Qafs) in the NE 1/4 section 4, T. 27 S., R. 9 W., Salt Lake Base Line and Meridian (SLBM), dips as steeply as 25° to the east even though the modern fan surface dips west (Figure 8). The discordant deposits may represent preserved slope-wash deposits that mantled an east-facing fault scarp formed along a strand of the OMF. Alternatively, the east-dipping Qafs could be cemented fan deposits that originally dipped west, but were later back-rotated to the east by faulting.

The most significant deposits of primary opaline sinter (Qs) are at Opal Mound along the southern end of the OMF, where laminated tan, red, white, and brown opaline sinter have a thickness of at least 5 m. Laminations are vertical along narrow, north-trending vents (Figure 9), but more commonly, the laminations dip gently away from the vents.

Hot spring mineral deposition along the OMF has been periodic and has likely spanned several thousand years. Discordant and/or elevated and dissected sinter-cemented alluvium is likely late Pleistocene in age. Cemented alluvium mapped on modern, undissected surfaces, such as the deposits found along the active drainage bottom in NMW (Kirby, 2019, Plate 1), are likely Holocene in age. Well 72-16, drilled 400 m east of Opal Mound (Figure 3), encountered sinter-cemented alluvium horizons at depths of 90 m and 130 m (Glenn and Hulen, 1979), indicating that additional aprons of sinter-cemented alluvium are interbedded with late Pleistocene fans (Qaf₂ and Qaf₃) on the OMF hanging wall. Faulder (1991) reported that paleomagnetic studies conducted at Opal Mound yielded a minimum age of 12,000 years for opal found there. Radiocarbon ages of ~1900 and ~1600 ¹⁴C yr B.P. reported by Lynne and others (2004, 2005) for the opal indicate that at least some opal deposition continued into the late Holocene, although spring activity at Opal Mound has not occurred historically.

Lacustrine Deposits

Lacustrine deposits are widely distributed in the central Milford Valley, and are exposed within 1.5 km to the west of the Utah FORGE site. The oldest exposed lacustrine deposit in the map area is a massive freshwater limestone (Qln) (Figure 10) that caps a series of low bluffs at an approximate elevation of 1510 m near the Beaver-Millard County line. The limestone is light tan to light gray and is partially covered by a thin veneer (<1 m thick) of gruss sourced from nearby alluvial fans. Several linear ground cracks, apparent in aerial photography and lidar-derived elevation models and observed in the field as vegetation lineaments (Figure 11), are developed on unit Qln in sections 1 and 12, T. 26. S., R. 10 W (SLBM). The origin of the cracks is unknown. We traced outcrops of the limestone northeast nearly to Antelope Spring in the Black Rock 7.5-minute quadrangle, where Oviatt (1991) mapped the unit as pre-Lake Bonneville lacustrine limestone. Hintze and Davis (2003) informally named this unit the “limestone of Twin Peaks,” and we apply this usage on our map. Although we have identified only a single 2- to 5-m-thick limestone bed in the map area, the limestone of Twin Peaks elsewhere commonly consists of several limestone beds interbedded with relatively soft marlstone that is up to 80 m thick (Zimmerman, 1961; Hintze and Davis, 2003). At Lava Ridge in the Black Point 7.5-minute quadrangle, the limestone of Twin Peaks is interbedded with basalt flows dated to about 2.5 Ma (Oviatt, 1991; Hintze and Davis, 2003). About 2.5 km southeast of Antelope Spring, limestone of Twin Peaks clearly overlies the ~1.3 Ma (Crecraft and others, 1981) Black Rock lava flow (Oviatt, 1991; this report), indicating that periodic limestone deposition by pre-Bonneville lakes spanned much of the early Pleistocene.



Figure 8. View to the south of east-dipping (~20°) sinter-cemented alluvium south of NMW; photo taken September 11, 2017.



Figure 9. View to the south of a spring vent on Opal Mound. White arrow points to hammer placed in the vent neck where banded opal is vertical. Note that opal laminations dip gently away from either side of the vent. Photo taken September 8, 2017.



Figure 10. Outcrop of pre-Lake Bonneville limestone (Qln) just south of the Millard-Beaver County line. The limestone is tentatively correlated with the limestone of Twin Peaks of Hintze and Davis (2003). Photo taken August 30, 2017.

Lake Bonneville began forming in the Great Salt Lake basin about 30 ka (Oviatt and others, 1992; Oviatt, 2015), but did not inundate the higher Sevier basin, Black Rock Desert, and Milford Valley until about 20 ka (Hintze and Davis, 2003). About 18 ka, Lake Bonneville reached its highest level, the Bonneville shoreline (Oviatt, 2015), at an elevation of about 1560 m in the map area. Prominent wave-cut escarpments formed on Qaf_{2,3} surfaces at the Bonneville shoreline reach a maximum height of about 6 m south of Ranch Canyon wash. Shortly after the highstand, failure of the Red Rock Pass threshold in southeastern Idaho caused a rapid drop of lake level to an elevation of 1445 m (Provo shoreline) (Hintze and Davis, 2003), which is well below the elevation of Milford Valley. During Lake Bonneville's approximately 2000 years of occupation in Milford Valley, wave action and currents extensively reworked the grass-dominated alluvial fans at and below the Bonneville shoreline. We mapped sand (map unit Qls) and gravel (Qlg) deposited in shore-zone beaches (Figure 12), spits, shoreline embankments, and cusped barrier beaches (v-bars). Fine-grained, deep-water lacustrine deposits consisting principally of silt, clay, and marl are common at lower elevations in the northwestern part of the map area.

QUATERNARY FAULTING

N. Mag Fault

The east-west-trending NMF is thought to play an important role in localizing the NMW canyon, and as a controlling structure for the RHS geothermal system (Nielson and others, 1978). The presence and geometry of the NMF is primarily based on displaced bedrock features (Petersen, 1975; Nielson and others, 1978) and geophysical data that indicate displacement is down to the south (Crebs and Cook, 1976; Ward and others, 1978). The fault may be pre-Quaternary (Simmons and others, 2016; this report), but a conspicuous east-west-trending scarp formed on late Pleistocene fan alluvium (Qaf₃) is near the inferred trace of the NMF, and therefore is discussed here. The north-facing, 1.5-km-long scarp is adjacent to, and closely parallels, the bottom of NMW, the linear toe of the Bailey Ridge lava flow, and the inferred trace of the NMF (Kirby, 2019). The discontinuous scarp faces uphill and is as much as 5 m high. Mapping by Nielson and others (1978), Sibbett and Neilson (1980), Rowley and others (2005), and Kirby (2019) show a north-dipping strand of the NMF associated with the scarp that implies late Pleistocene surface faulting. We found no additional scarps formed on Qaf₃ deposits or bedrock to the west or east along the inferred trace of the NMF.



Figure 11. One of several vegetation lineaments just south of the Millard-Beaver County line that mark ground cracks formed on the underlying limestone of Twin Peaks (Qln); photo taken September 25, 2017.

Figure 13 presents an alternative interpretation that explains the scarp in NMW as resulting from differential erosion along a geologic contact rather than due to surface faulting. The scarp is formed on grass- and obsidian-rich alluvium identical to Qaf₃ alluvium that forms the broad fan surface underlying the Blundell power plant. The scarp appears to be a remnant of this once-continuous Qaf₃ fan that extended up NMW and abutted against the 0.8-Ma Bailey Ridge lava flow and the north canyon wall. Later incision of NMW in latest Pleistocene to Holocene time along the toe of the Bailey Ridge lava flow isolated a remnant of the Qaf₃ fan along the northern canyon wall. Erosion along the linear contact between the more resistant Qaf₃ remnant and adjacent slope-wash (Qafy) deposits on the canyon wall (Figure 13), rather than surface faulting, may have formed the north-facing scarp. Brogan and Birkhahn (1981) also suggested that erosion along a geologic contact may be responsible for the scarp.

The prominent line of sinter deposits that delineates the north-south-trending OMF (discussed in next section) appears to be undeflected by the intersecting NMF (Kirby, 2019, Plate 1), indicating that the NMF is the older structure. If scarp formation on late Pleistocene alluvium in NMW is non-tectonic in origin, then the latest movement on the NMF was likely pre-Quaternary since the fault is in an unfavorable orientation to accommodate east-west Basin and Range extension (Nielson, 1989; Faulder, 1994).



Figure 12. View to the east into a sand and gravel pit excavated into a Lake Bonneville shoreline beach deposit east of Milford (SW1/4 section 9, T. 28 S., R. 10 W. [SLBM]); photo taken August 30, 2017.

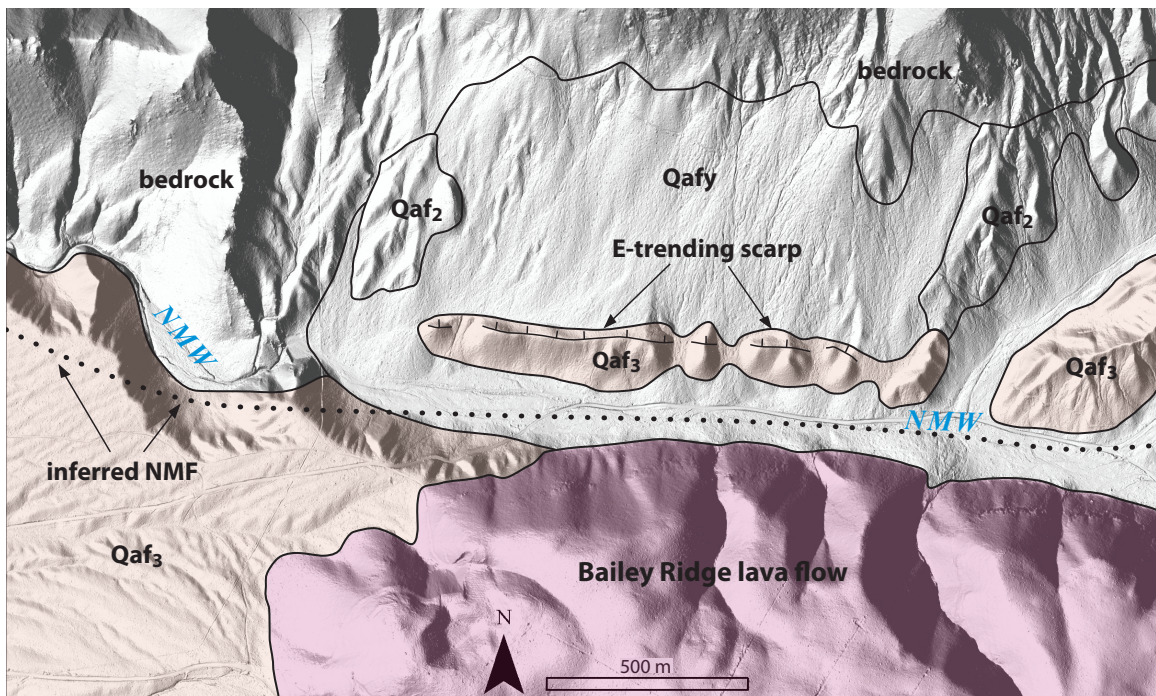


Figure 13. Lidar-derived hillshade image of a prominent east-trending scarp oriented parallel to NMW and the toe of the Bailey Ridge lava flow. This geologic mapping varies from the mapping of Kirby (2019) and presents an alternative interpretation of the relation between the east-trending scarp and the NMF. Qaf_3 , Qaf_2 =old (late Pleistocene) fan alluvium, Qaf_y =young (Holocene to latest Pleistocene) fan alluvium and slope wash.

Opal Mound Fault

The north-northeast-striking OMF extends for at least 7 km near the western margin of the Mineral Mountains (Figure 3). The OMF dips east toward the Mineral Mountains and defines the western boundary of the RHS geothermal area (Nielson and others, 1978, 1986; Faulder, 1991). Near NMW, the OMF consists of both east- and west-dipping splays (Figure 14). The fault is up to 1.5 km distant from the Mineral Mountains range front. Scarp height varies widely from about 18 m where the fault juxtaposes units Taf and Qaf₃ southwest of the power plant, to 0 m where the scarp has been removed by erosion (Figure 4). Burial ages (IRSL) from fault-isolated alluvial-fan deposits (Qaf₃) just west of the OMF indicate aggradation west of the OMF ceased at about 56 ka (Figure 14). Scarps measured in alluvium along the 7 km fault length averaged ~11 m high with an average slope of ~6° (Kleber and others, 2017).

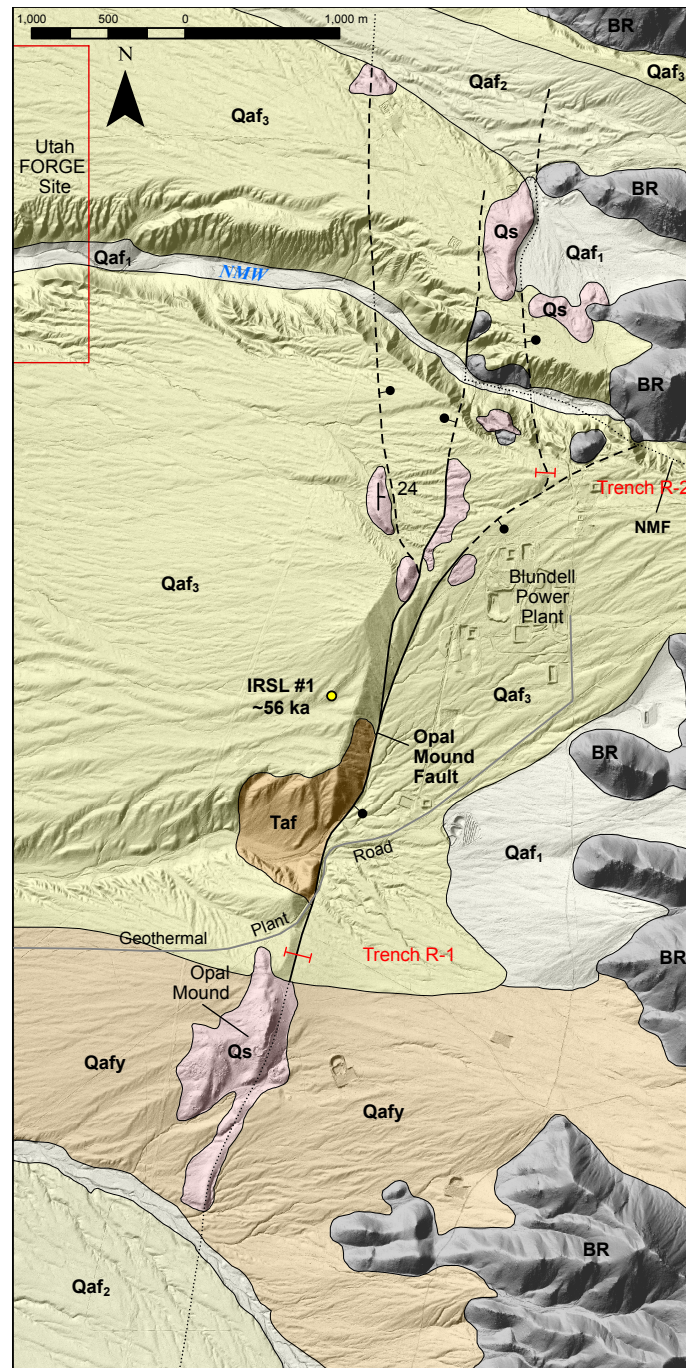


Figure 14. Simplified Quaternary geology on a lidar-derived hillshade image of the area near the OMF. Taf=late Tertiary basin-fill deposits; Qaf₃, Qaf₂=late Pleistocene alluvial fans; Qaf₁=latest Pleistocene to Holocene alluvial fans; Qaf_y=undivided young (Holocene to late Pleistocene) fan alluvium; Qs=primary siliceous sinter and sinter-cemented alluvium, undivided; BR=bedrock.

Hot springs have periodically emanated from fissures along the OMF and have resulted in the deposition of primary, laminated opaline sinter and cementation of adjacent alluvium. Hot spring mineral deposition has been contemporaneous with faulting along the OMF. As previously discussed in the Hot Spring Deposits section, buried horizons of sinter-cemented fan alluvium east of the OMF and the possible fault-rotated sinter-cemented alluvium indicate that some older spring deposits have been displaced by the fault. Previous workers have suggested that primary banded opal as young as about 1.6 kyr (Lynne and others, 2004, 2005) exposed on the surface at Opal Mound is displaced by the OMF (e.g., Petersen, 1975; Lynne and others, 2005). However, we could not find evidence for the displacement of either sinter or alluvium of Holocene age along the OMF. A reconnaissance investigation of the OMF by Anderson and Bucknam (1979) likewise failed to find evidence for Holocene faulting. We believe that if resistant siliceous sinter deposits were displaced by surface faulting on the OMF in the Holocene, fault scarps would be easily detected in both high-resolution (0.5 m) lidar elevation data and in the field. It is more likely that the youngest (Holocene) sinter deposits were sourced from vents along the crest of Opal Mound and that they simply drape over a preexisting scarp and are unbroken by the underlying OMF. Likewise, recent mapping (see Kirby, 2019, Plate 1) shows that young, mostly Holocene, alluvial deposits cover the OMF at many locations and that the deposits are not displaced.

Paleoseismic Data

Paleoseismic trench logs are available from a 1981 Woodward–Clyde study completed for the U.S. Geological Survey investigating faults and geothermal anomalies in the Great Basin (Brogan and Birkhahn, 1981). Woodward–Clyde excavated a paleoseismic trench (R-1) near the intersection of Geothermal Plant Road and the southern end of the OMF (Figure 14). Depositional units exposed included older bedded alluvium, colluvium, mudflows, and younger alluvium (Figure 15). There was evidence that hydrothermal fluids had circulated within more permeable parts of a mudflow. Dames and Moore identified a 10-m-wide fault zone in the trench. The fault zone had apparent down-to-the-east movement, cemented shear fabrics, and discrete normal-sense displacements of 5–33 cm. Trench R-2, excavated across a suspected fault scarp just south of NMW (Figure 14), exposed an unfaulted zone of older alluvium.

We interpret that scarp development along the OMF is largely influenced by differential erosion of resistant, siliceous sinter exposed along the fault. The steeper, most prominent scarps are coincident with significant spring deposits and resemble fault-line scarps (Figure 14). Similarly, a well-defined scarp north of Opal Mound formed where the OMF juxtaposes rela-

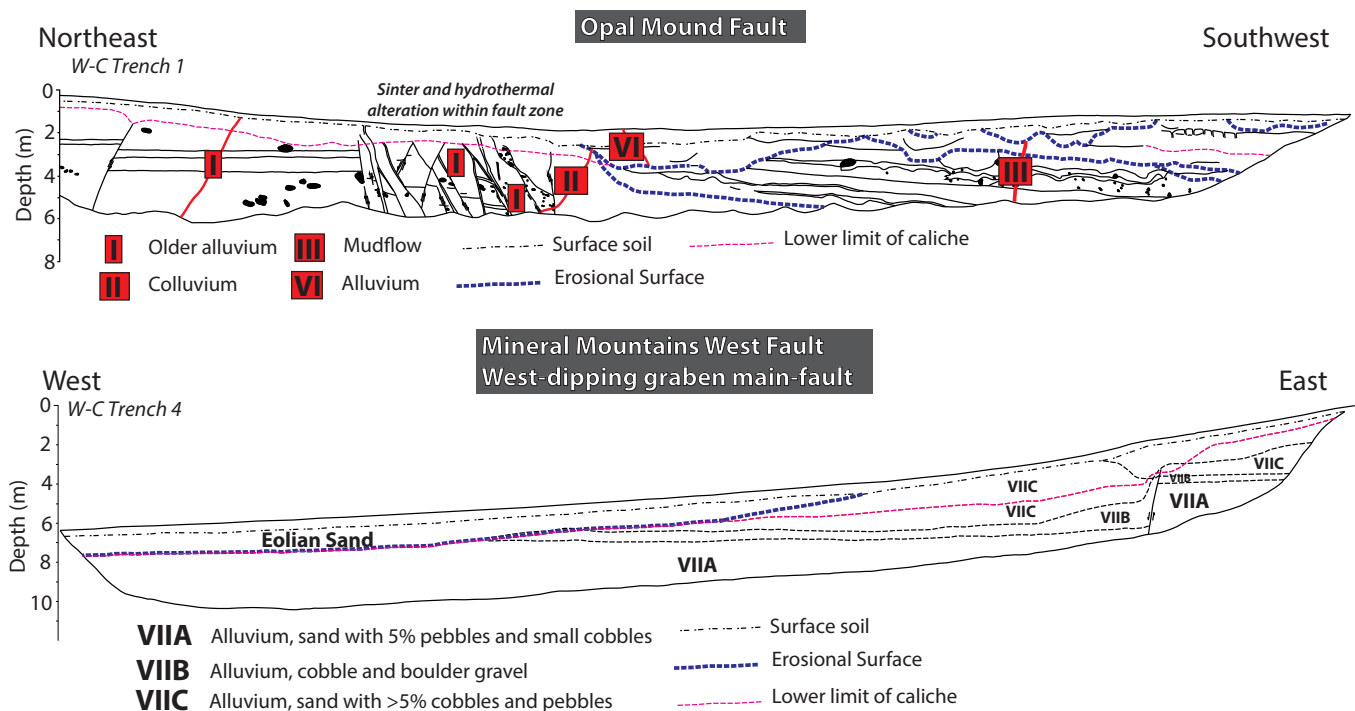


Figure 15. Reproduced paleoseismic trench logs from Woodward–Clyde investigation (Brogan and Birkhahn, 1981). Approximate trench locations are on Figure 3. Trench 1 was excavated on the OMF and trench 4 was on a strand of the MMWFZ. No geochronology samples were analyzed.

tively resistant late Neogene basin-fill deposits (Taf) with grussy Qaf₃ deposits (Figure 14). Relatively steep escarpments, particularly near Opal Mound, have formed on both the east and west sides of north-trending spring vents adjacent to the fault (Figure 14). If scarps near Opal Mound were formed only by surface faulting along the east-dipping OMF, we would expect to see scarp formation only on the east side of the spring deposits. Where not armored by sinter deposits, the OMF scarp has either been degraded by erosion to a very low angle or has been completely removed. One of the few OMF scarps not influenced by spring deposits is formed solely on alluvial-fan deposits in the NW corner of section 9, T. 27 S., R. 9 W. (SLBM) (Kirby, 2019, Plate 1). There, the scarp has degraded to a gentle 4° slope angle.

Spring deposits are generally absent along a 1-km-long section of the OMF near NMW—this section also lacks any detectable topographic expression of the fault (Figure 14). Additionally, several west-flowing drainages, including minor drainages with drainage basins less than 1.5 km², pass through the OMF scarp (Figure 14), indicating significant time has elapsed since the most recent surface displacement on the fault (Petersen, 1975). Where not influenced by sinter deposits, the morphology and degree of dissection of the OMF scarp appear more mature than Bonneville shoreline scarps formed on alluvial-fan material of similar age and texture. Figure 16 shows scarp height plotted against scarp slope measured along the OMF and the MMWFZ (discussed in next section) in the study area. We did not measure scarps formed on sinter or opal deposits. Scarp profile data from regional Basin and Range faults (Anderson and Bucknam, 1979) are included on the graph for comparison. The graph shows that the OMF scarp has a significantly lower slope than other regional Basin and Range faults and the MMWFZ (Figure 16).

Based on cross-cutting relations with both late Pleistocene and Holocene alluvial deposits, IRSL ages from fault-isolated fan deposits, degree of dissection, scarp slope degradation, development of through-going drainages, and the development of fault-line scarp morphology, we deduce a late Pleistocene age for the most recent movement on the OMF.

Mineral Mountains West Faults

Movement on a complex zone of north-south-trending normal faults has formed a series of scarps on late Pleistocene alluvial fans (map units Qaf₂ and Qaf₃) (see Kirby, 2019, Plate 1; Figure 17) about midway between the Mineral Mountains range front and the Bonneville shoreline. The fault zone begins near the southern boundary of the Utah FORGE site, where it consists of several west- and east-dipping strands, and continues south for about 40 km to near Minersville (Rowley and others, 2005; Figure 2). There are no definitively mapped fault scarps within the Utah FORGE site. The fault zone is named the Mineral Mountains (West Side) faults in the *Quaternary Fault and Fold Database of the United States* (U.S. Geological Survey, 2018) and the *Utah Quaternary Fault and Fold Database* (Utah Geological Survey, 2018). We simplify this name to the Mineral Mountains West fault zone (MMWFZ).

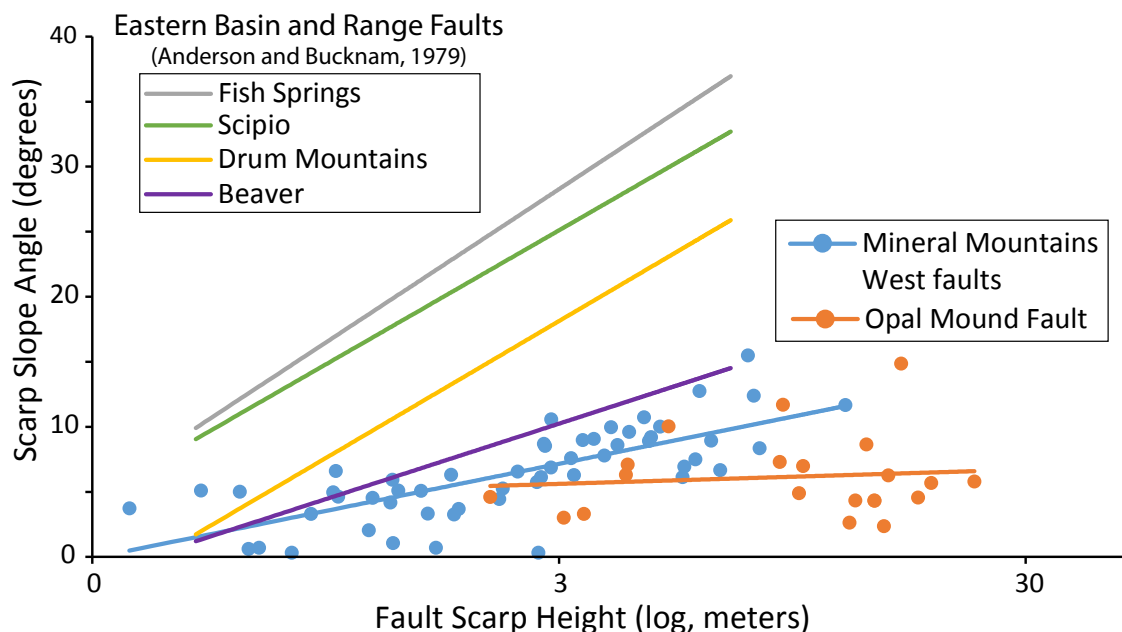


Figure 16. Scarp height (log, meters) plotted against scarp slope (degrees) measured on MMWF faults and the OMF with a logarithmic regression. Regression functions from other Basin and Range faults are from Anderson and Bucknam (1979).



Figure 17. Low-sun angle (a.m.) photo of a low MMWFZ scarp (<5 m high) formed on late Pleistocene alluvial-fan deposits north of Ranch Canyon. The Mineral Mountains range front is 2 km distant from the scarp. View is to the southeast; photo taken September 11, 2017.

Scarps associated with the multi-strand MMWFZ south of the FORGE site have a mean height of 3.5 m and some are less than 1.5 m high. The faults form a prominent graben that varies in width from ~700 to 1200 m with internal horst and graben blocks. Throughout the graben, the highest and most continuous scarps are west-dipping and displace alluvial deposits 1 to 8 m with a normal sense of motion. Within the graben, east-dipping scarps have an average height and slope of 3.18 m and 5°, respectively, and west-dipping faults have an average height and slope of 3.16 m and 7°, respectively. Both east- and west-dipping scarps increase in height and slope south of the FORGE site. South of Corral Canyon, multiple strands of the fault converge into a single fault that has produced a scarp as high as 13 m (Figure 7). The larger average displacement on the fault south of Corral Canyon has resulted in higher rates of erosion on the upthrown Qaf_{2,3} fan surface. Substantial alluvium (Qaf₁, Qaf_y) derived from the upthrown block has buried much of the downthrown Qaf_{2,3} surface south of Corral Canyon and conceals the MMWFZ (Kirby, 2019, Plate 1).

Brogan and Birkhahn (1981) and Rowley and others (2005) mapped short faults (<2 km long) several kilometers west of the MMWFZ in central Milford Valley, where they possibly displace Lake Bonneville deposits. Our mapping produced no evidence for fault-displaced Lake Bonneville sediment.

Paleoseismic Data

Paleoseismic data are available for two trenches excavated on MMWFZ graben faults by Brogan and Birkhahn (1981). Trench R-3 crossed a prominent east-dipping graben fault north of Ranch Canyon (Kirby, 2019, Plate 1; Figure 3). The trench exposed a series of mudflows displaced about 0.5 m down-to-the-east. Trench R-4, excavated across a west-dipping graben fault about 2 km north of trench R-3 (Kirby, 2019, Plate 1; Figure 3), exposed alluvium interpreted to be intermediate in age with the older alluvium exposed in trench R-1 across the OMF. Brogan and Birkhahn (1981) identified 2.2 m of down-to-the-west displacement of alluvium in trench R-4 (Figure 15), but did not interpret the number of surface-faulting earthquakes associated with these displaced deposits. After reviewing the R-4 trench log, we interpret the presence of at least one, and possibly two scarp-derived colluvial wedges, providing evidence for one or two surface-rupturing earthquakes on this strand of the MMWFZ. Trench R-4 is within a complicated graben, and there are several other east- and west-facing graben faults close to this site that may complicate interpretations of the number of earthquakes and the amount of slip-per-earthquake for the entire fault zone.

MMWFZ scarps are deeply dissected, locally discontinuous, and generally display similar scarp morphologies as nearby Bonneville shorelines that formed about 18 ka. Latest Pleistocene to Holocene alluvial deposits (map unit Qaf₁) have filled several grabens and other low areas adjacent to the MMWFZ. The young alluvium conceals the faults and has not been displaced. Although the MMWFZ is the major western range-bounding fault for the Mineral Mountains, Quaternary slip

rates on the fault zone in the map area have been insufficient to form a range front; the mountain front lies 3 to 5 km to the east. We deduce a latest Pleistocene age for the most recent surface faulting on the MMWFZ.

SUMMARY OF LATE NEOGENE TO QUATERNARY GEOLOGY

Uplift and maximum relief of the Mineral Mountains likely occurred in late Miocene to Pliocene time (Evans and Nielson, 1982; Machette, 1985; Coleman and others, 2001). Erosion of the rapidly uplifting mountain block resulted in coarse sedimentation into the incipient Milford Valley. Erosion of the Mineral Mountains block continued into the early Pleistocene, forming deeply embayed canyons and other gently dipping erosional surfaces that graded to the adjacent valley floor. At least one early Pleistocene freshwater lake occupied the central part of Milford Valley and deposited limestone. Starting in the early middle Pleistocene (~0.8 Ma), volcanism along the crest of the Mineral Mountains deposited rhyolitic lava flows that partially filled NMW, Wildhorse, and Ranch Canyons. By late-middle Pleistocene time, alluvial fans began aggrading eastward into the Mineral Mountains, resulting in the burial of low-relief bedrock foothills and the partial infilling of the deeply embayed canyons. In NMW, the aggrading fans lapped against the toe of the ~0.8-Ma Bailey Ridge lava flow. In late Pleistocene time, movement on the OMF and the MMWFZ displaced alluvial-fan surfaces several meters but were not sufficiently active to form mountain fronts. The east-dipping OMF is in a favorable position and orientation to form the western boundary of the RHS geothermal system. Periodic hot spring activity throughout the late Pleistocene and into the Holocene deposited abundant siliceous sinter along the OMF. Differential erosion of the sinter deposits has greatly influenced the OMF's scarp morphology. Sand and gravel at the distal ends of coalesced alluvial fans were extensively reworked—locally, into prominent barrier bars and v-embankments—by late Pleistocene Lake Bonneville, which occupied Milford Valley from about 20 to 18 ka. Perhaps driven by local uplift, or the lowering of base level following the recession of Lake Bonneville (~18 ka), NMW, Ranch Canyon, Corral Canyon, and the Beaver River incised their channels, thus rendering many fan surfaces inactive. This period of incision contributed to latest Pleistocene to Holocene deposition of alluvium near the mouths of the entrenched drainages, where the deposits obscure and bury the Bonneville shoreline. Latest Pleistocene to Holocene deposits, including opaline sinter and young alluvium, locally conceal the OMF and MMWFZ and are not faulted. A highly degraded and dissected OMF scarp morphology indicates a late Pleistocene age for the most recent surface displacement. Scarp morphologies of the MMW fault zone appear younger than those of the OMF, and are similar to those formed by Lake Bonneville shorelines (~18 ka), indicating a latest Pleistocene age for most recent movement on the MMW fault zone.

ACKNOWLEDGMENTS

We would like to thank Dr. Tammy Rittenour, Michelle Nelson, and Carlie Ideker of Utah State University (USU) for assistance with sample collection in the field and sample processing at the USU Luminescence lab (<http://www.usu.edu/geo/luminlab/>). We would also like to thank Brendon Quirk of the University of Utah for his insights on dating methods and processing. Reviews from William Lund, Michael Hylland, and Stephanie Carney of the Utah Geological Survey contributed to this manuscript.

REFERENCES

- Anderson, R.E., and Bucknam, R.C., 1979, Map of fault scarps in unconsolidated sediments, Richfield 1° x 2° quadrangle, Utah: U.S. Geological Survey Open-File Report 79-1236, 15 p., scale 1:250,000.
- Brogan, G., and Birkhahn, P., 1981, Faults and occurrence of geothermal anomalies: Woodward-Clyde Consultants final report to the U.S. Geological Survey Geothermal Research Program, Contract 14-08-0001-16310, variously paginated.
- Crebs, T.J., and Cook, K.L., 1976, Technical report—gravity and ground magnetic surveys of the central Mineral Mountains, Utah, volume 6, final report: unpublished report prepared by Department of Geology and Geophysics, University of Utah, Salt Lake City, 129 p.
- Crecraft, H.R., Nash, W.P., and Evans, S.H., Jr., 1981, Late Cenozoic volcanism at Twin Peaks, Utah, geology and petrology: *Journal of Geophysical Research*, v. 86, p. 10,303–10,320.
- Coleman, D.S., Walker, J.D., Bartley, J.M., and Hodges, K.V., 2001, Thermochronologic evidence for footwall deformation during extensional core complex development, Mineral Mountains, Utah, *in* Erskine, M.C., Faulds, J.E., Bartley, J.M., and Rowley, P.D., editors, *The geologic transition, High Plateaus to Great Basin—a symposium and field guide* (The

- Mackin Volume): Utah Geological Association and Pacific Section of the American Association of Petroleum Geologists, Utah Geological Association Publication 30, p. 155–168.
- Dickinson, W.R., 2006, Geotectonic evolution of the Great Basin: *Geosphere*, v. 2, p. 353–368, doi: 10.1130/GES00054.1.
- DuRoss, C., in preparation, Scarp offset v4g, MATLAB script.
- Evans, S.H., Jr., and Nielson, D.L., 1982, Thermal and tectonic history of the Mineral Mountains intrusive complex: *Geothermal Resources Council Transactions*, v. 6, p. 15–18.
- Faulder, D.D., 1991, Conceptual geologic model and native state model of the Roosevelt Hot Springs hydrothermal system: *Proceedings, 16th Workshop on Geothermal Reservoir Engineering*, Stanford University, p. 131–142.
- Faulder, D.D., 1994, Long-term flow test #1, Roosevelt Hot Springs, Utah: *Geothermal Resources Council Transactions*, v. 18, p. 583–590.
- Faulds, J.E., Hinz, N.H., Coolbaugh, M.F., Cashman, P.H., Kratt, C., Dering, G., Edwards, J., Mayhew, B., and McLachlan, H., 2011, Assessment of favorable structural settings of geothermal systems in the Great Basin, Western USA: *Geothermal Resources Council Transactions*, v. 35, p. 777–783.
- Hintze, L.F., and Davis, F.D., 2003, *Geology of Millard County, Utah*: Utah Geological Survey Bulletin 133, 305 p.
- Hintze, L.F., Davis, F.D., Rowley, P.D., Cunningham, C.G., Steven, T.A., and Willis, G.C., 2003, *Geologic map of the Richfield 30' x 60' quadrangle, southeast Millard County, and parts of Beaver, Piute, and Sevier Counties, Utah*: Utah Geological Survey Map 195, scale 1:62,500.
- Glenn, W.E., and Hulen, J.B., 1979, Interpretation of well log data from four drill holes at Roosevelt Hot Springs KGRA: unpublished report prepared by Earth Science Laboratory, University of Utah Research Institute, Salt Lake City, Utah, for U.S. Department of Energy, Division of Geothermal Energy, 74 p.
- Kirby, S.M., 2019, Revised mapping of bedrock geology adjoining the Utah FORGE site, in Allis, R., and Moore, J.N., editors, *Geothermal characteristics of the Roosevelt Hot Springs system and adjacent FORGE EGS site*, Milford, Utah: Utah Geological Survey Miscellaneous Publication 169-A, 6 p., 2 plates, scale 1:24,000, <https://doi.org/10.34191/MP-169-A>.
- Kleber, E., Kirby, S.M., Hiscock, A.I., and Bowman, S., 2017, Preliminary assessment of Quaternary faulting based on high resolution topographic data near the FORGE geothermal site, Mineral Mountains, Utah, USA: *Proceedings for the 8th international INQUA Meeting on Paleoseismology, Active Tectonics and Archaeoseismology (PATA)*, November 12–15, 2017, New Zealand.
- Lipman, P.W., Rowley, P.D., Mehnert, H.H., Evans S.H., Jr., Nash, W.P., and Brown F.H., 1978, Pleistocene rhyolite of the Mineral Mountains, Utah—geothermal and archeological significance: *U.S. Geological Survey Journal of Research*, v. 6, p. 133–147.
- Lynne, B.Y., Campbell, K.A., Moore, J.N., and Browne, P.R.L., 2004, Siliceous sinter diagenesis at the Opal Mound, Roosevelt Hot Springs, Utah, USA: *Proceedings, 26th New Zealand Geothermal Workshop*, p. 12–17.
- Lynne, B.Y., Campbell, K.A., Moore, J.N., and Browne, P.R.L., 2005, Diagenesis of 1900 year-old siliceous sinter (opal-A to quartz) at Opal Mound, Roosevelt Hot Springs, Utah: *Sedimentary Geology*, v. 179, p. 249–278.
- Machette, M.N., 1985, Late Cenozoic geology of the Beaver Basin, southwestern Utah: *Brigham Young University Geology Studies*, v. 32, pt. 1, p. 19–37.
- Mower, R.W., and Cordova, R.M., 1974, Water resources of the Milford area, Utah, with emphasis on ground water: Utah Department of Natural Resources Technical Publication no. 43, 99 p.
- Nielson, D.L., 1989, Stress in geothermal systems: *Geothermal Resources Council Transactions*, v. 13, p. 271–276.
- Nielson D. L., Evans, S.H., Jr., and Sibbett, B.S., 1986, Magmatic, structural, and hydrothermal evolution of the Mineral Mountains intrusive complex, Utah: *Geological Society of America Bulletin*, v. 97, no. 6, p. 765–777.
- Nielson, D.L., Sibbett, B.S., McKinney, D.B., Hulen J.B., Moore, J.N., and Samberg, S.M., 1978, *Geology of Roosevelt Hot Springs KGRA, Beaver County, Utah*: unpublished report prepared by Earth Science Laboratory, University of Utah Research Institute, Salt Lake City, Utah, for U.S. Department of Energy, Division of Geothermal Energy, 120 p.
- Oviatt, C.G., 1991, Quaternary geology of the Black Rock Desert, Millard County, Utah: Utah Geological and Mineral Survey Special Study 73, 23 p., scale 1:100,000.
- Oviatt, C.G., 2015, Chronology of Lake Bonneville, 30,000 to 10,000 yr B.P.: *Quaternary Science Review*, v. 110, p. 166–171.
- Oviatt, C.G., Currey, D.R., and Sack, D., 1992, Radiocarbon chronology of Lake Bonneville, eastern Great Basin, USA: *Palaeogeography, Palaeoclimatology, Palaeoecology*, v. 99, p. 225–241.

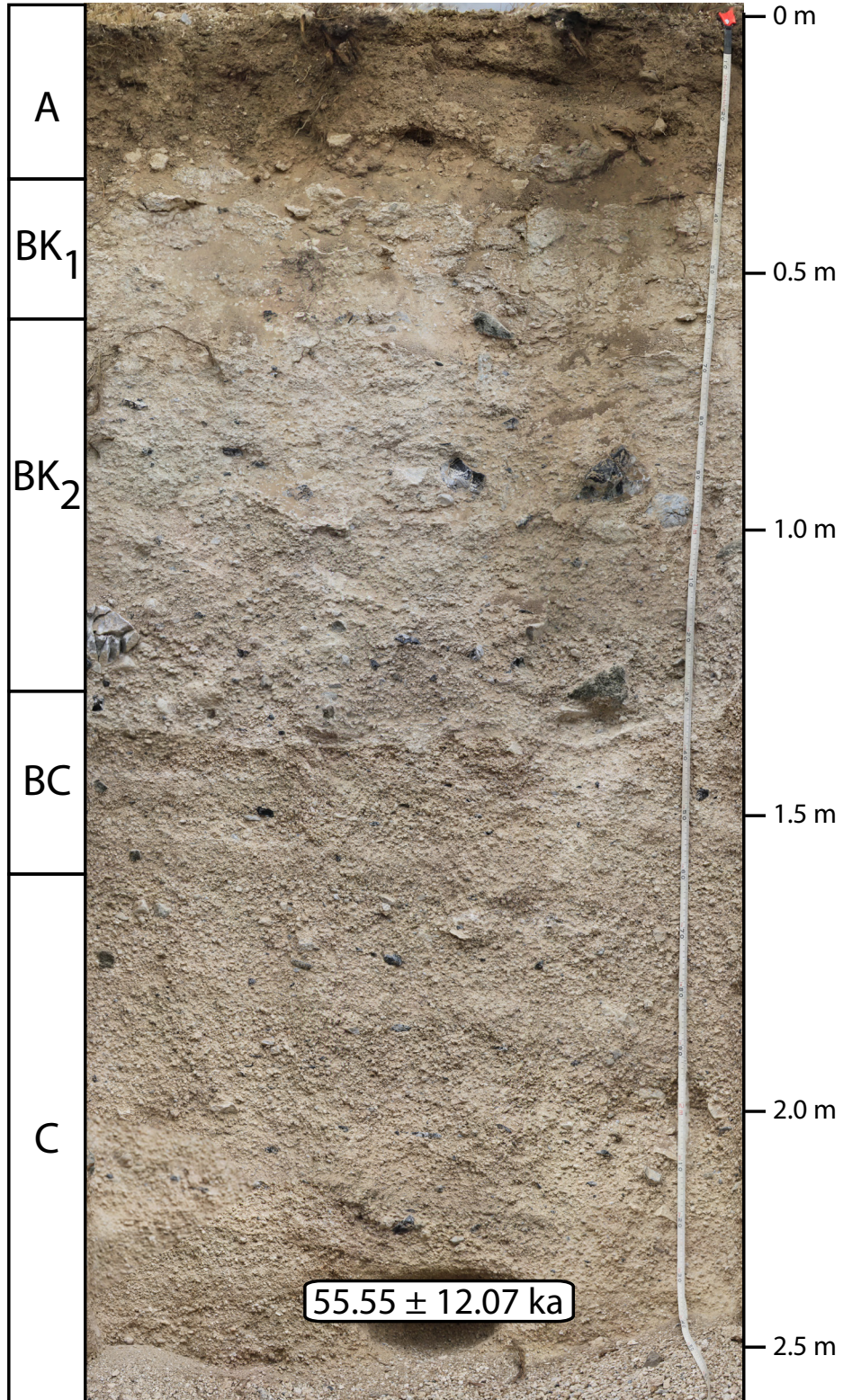
- Petersen, C.A., 1975, Geology of the Roosevelt Hot Springs area, Beaver County, Utah: *Utah Geology*, v. 2, no. 2, p. 109–116.
- Rhodes, E.J., 2011, Optically stimulated luminescence dating of sediments over the past 200,000 years: *Annual Review of Earth and Planetary Sciences*, v. 39, p. 461–488.
- Rittenour, T.M., 2008, Luminescence dating of fluvial deposits: applications to geomorphic, paleoseismic, and archaeological research: *Boreas*, v. 37, p. 613–635.
- Rowley, P.D., Vice, G.E., McDonald, R.E., Anderson, J.J., Machette, M.N., Maxwell, D.J., Ekren, E.B., Cunningham, C.G., Steven, T.A., and Wardlaw, B., 2005, Interim geologic map of the Beaver 30' x 60' quadrangle, Beaver, Piute, Iron, and Garfield Counties, Utah: Utah Geological Survey Open-File Report 454, 27 p., 1 plate, scale 1:100,000.
- Sibbett, B.S., and Nielson, D.L., 1980, Geology of the central Mineral Mountains, Beaver County, Utah: University of Utah Research Institute, Earth Science Laboratory Report 33, 42 p. (under DOE contract no. DE-AC07-78ET28392).
- Simmons, S., Kirby, S., Jones, C., Moore, J., Allis, R., Brandt, A., and Nash, G., 2016, The geology, geochemistry, and geohydrology of the FORGE deep well site, Milford, Utah: *Proceedings, 41st Workshop on Geothermal Reservoir Engineering*, 10 p.
- Stahl, T., and Niemi, N.A., 2017, Late Quaternary faulting in the Sevier Desert driven by magmatism: *Scientific Reports*, v. 7, article no. 44372, doi: 10.1038/srep44372.
- Utah Geological Survey, 2018, Utah Quaternary fault and fold database: Online, <https://geology.utah.gov/resources/data-databases/qfaults/>.
- U.S. Geological Survey, 2018, Quaternary fault and fold database of the United States: U.S. Geological Survey Earthquake Hazards Program, Online, <https://earthquake.usgs.gov/hazards/qfaults/>.
- Ward, S.H., Parry, W.T., Nash, W.P., Sill, W.R., Cook, K.L., Smith, R.B., Chapman, D.S., Brown, F.H., Whelan, J.A., and Bowman, J.R., 1978, A summary of the geology, geochemistry, and geophysics of the Roosevelt Hot Springs thermal area, Utah: *Geophysics*, v. 43, p. 1515–1542.
- Zimmerman, J.T., 1961, Geology of the Cove Creek area, Millard and Beaver Counties, Utah: Salt Lake City, University of Utah, M.S. thesis, 91 p., scale 1:24,000.

Appendix A: IRSL Soil Pit Logs by E. Kleber

IRSL Site 1 (USU-2680)

Sampled August 23, 2017

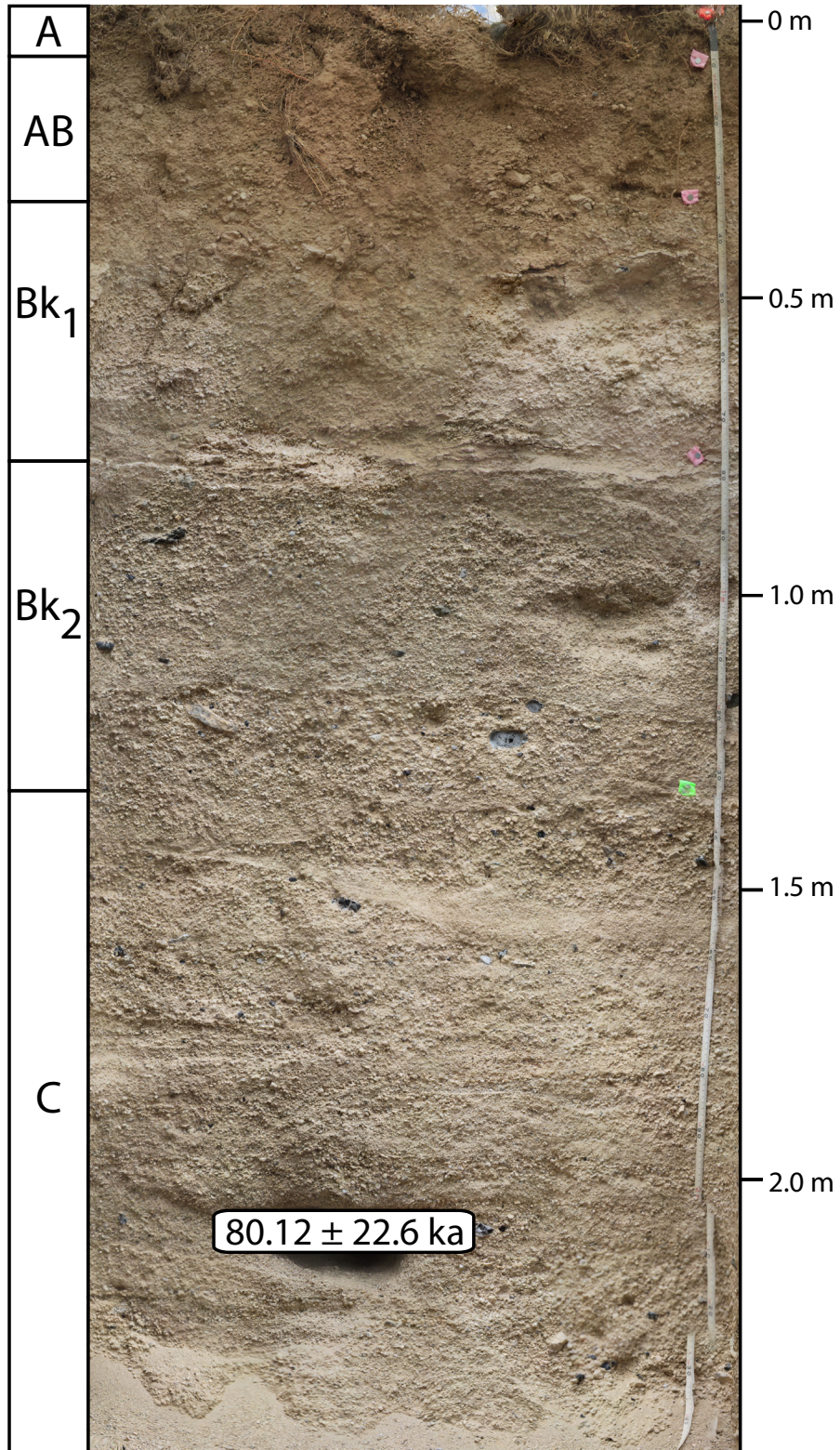
N 38.48468, W 112.86554, 1800 m ASL



IRSL Site 2 (USU-2681)

Sampled August 23, 2017

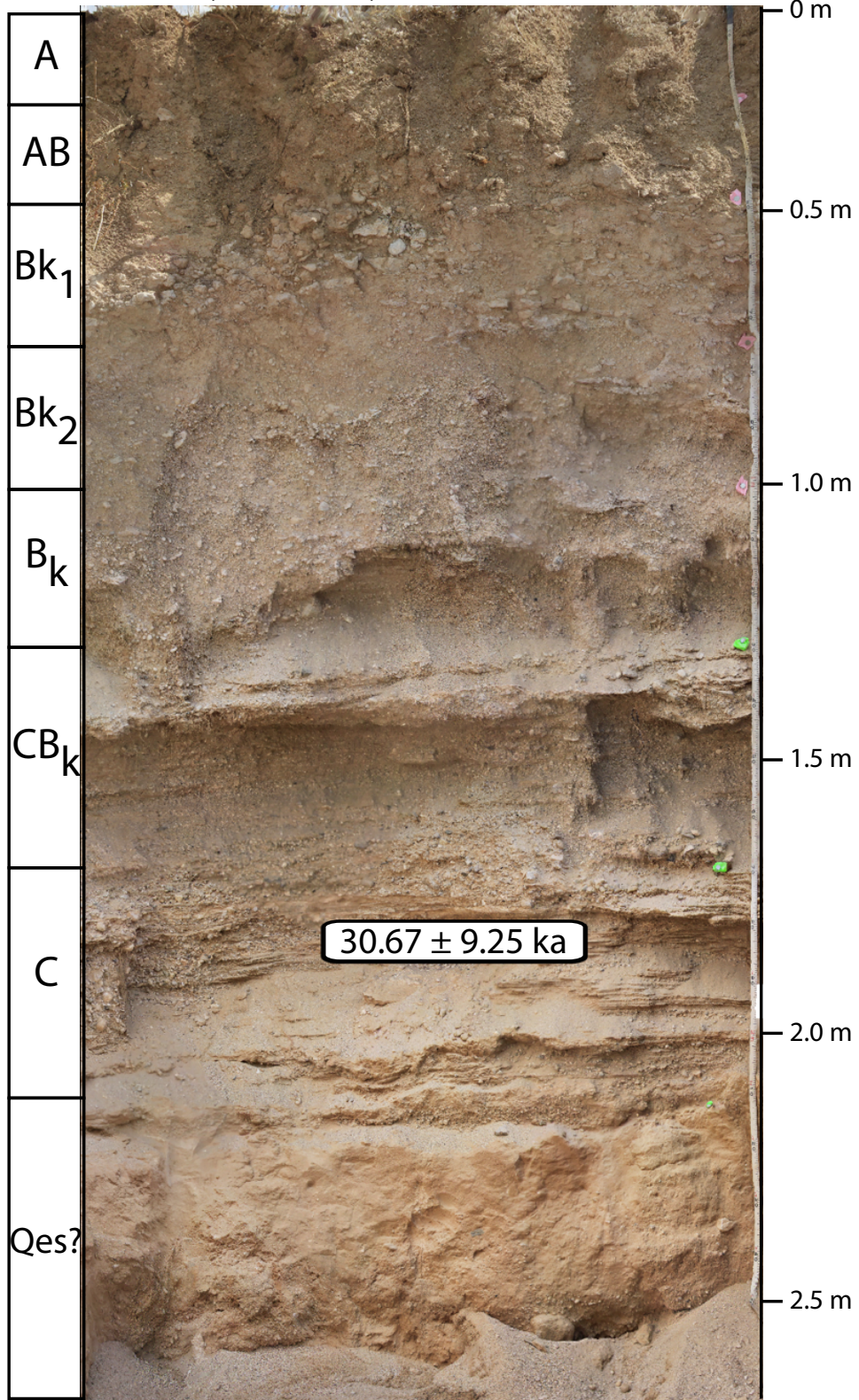
N 38.48514, W 112.88897, 1703 m ASL



IRSL Site 3 (USU-2683)

Sampled August 23, 2017

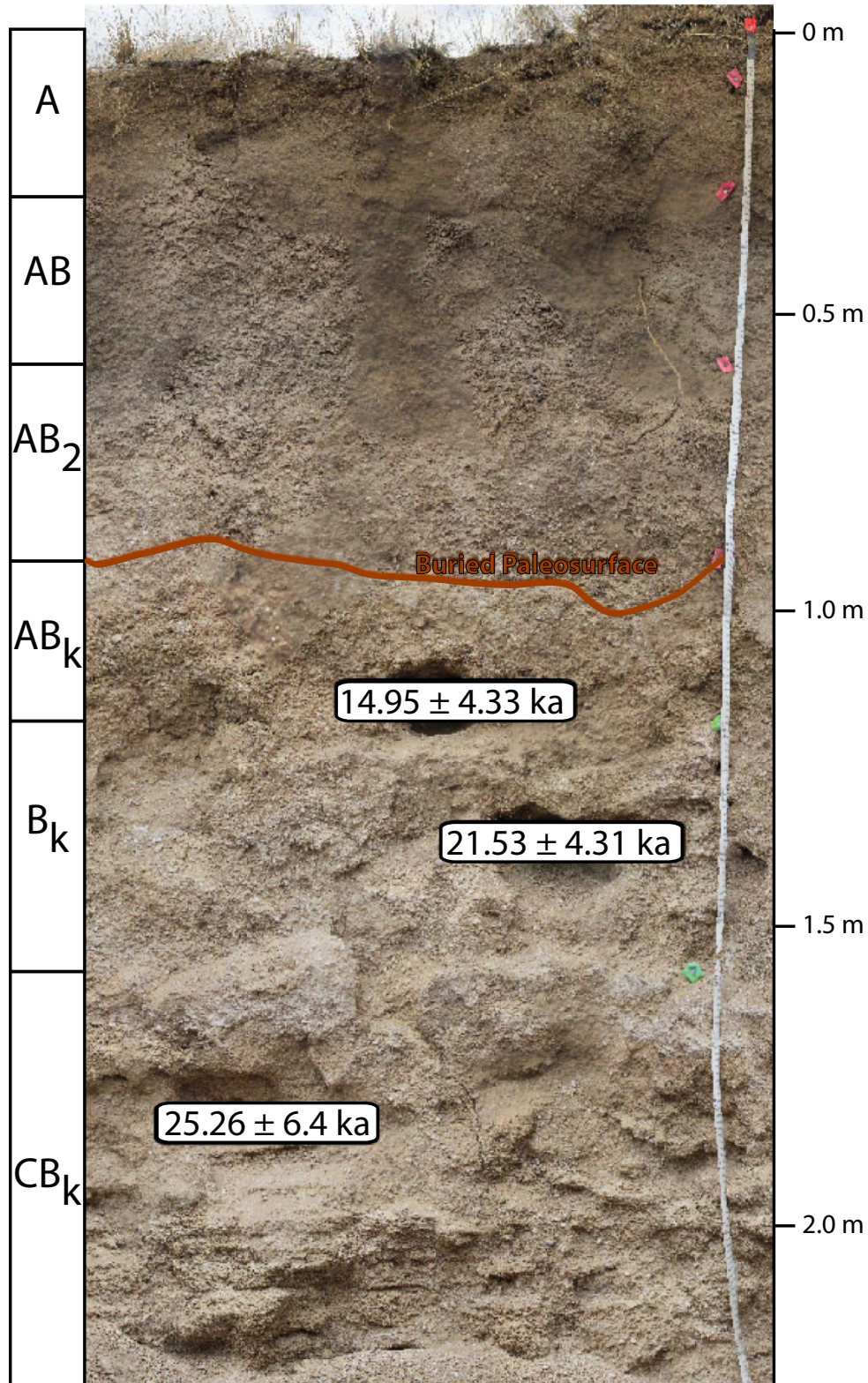
N 38.43803, W 112.90150, 1171 m ASL



IRSL Site 4a (USU-2684, 2685, 2686)

Sampled August 23 and 24, 2017

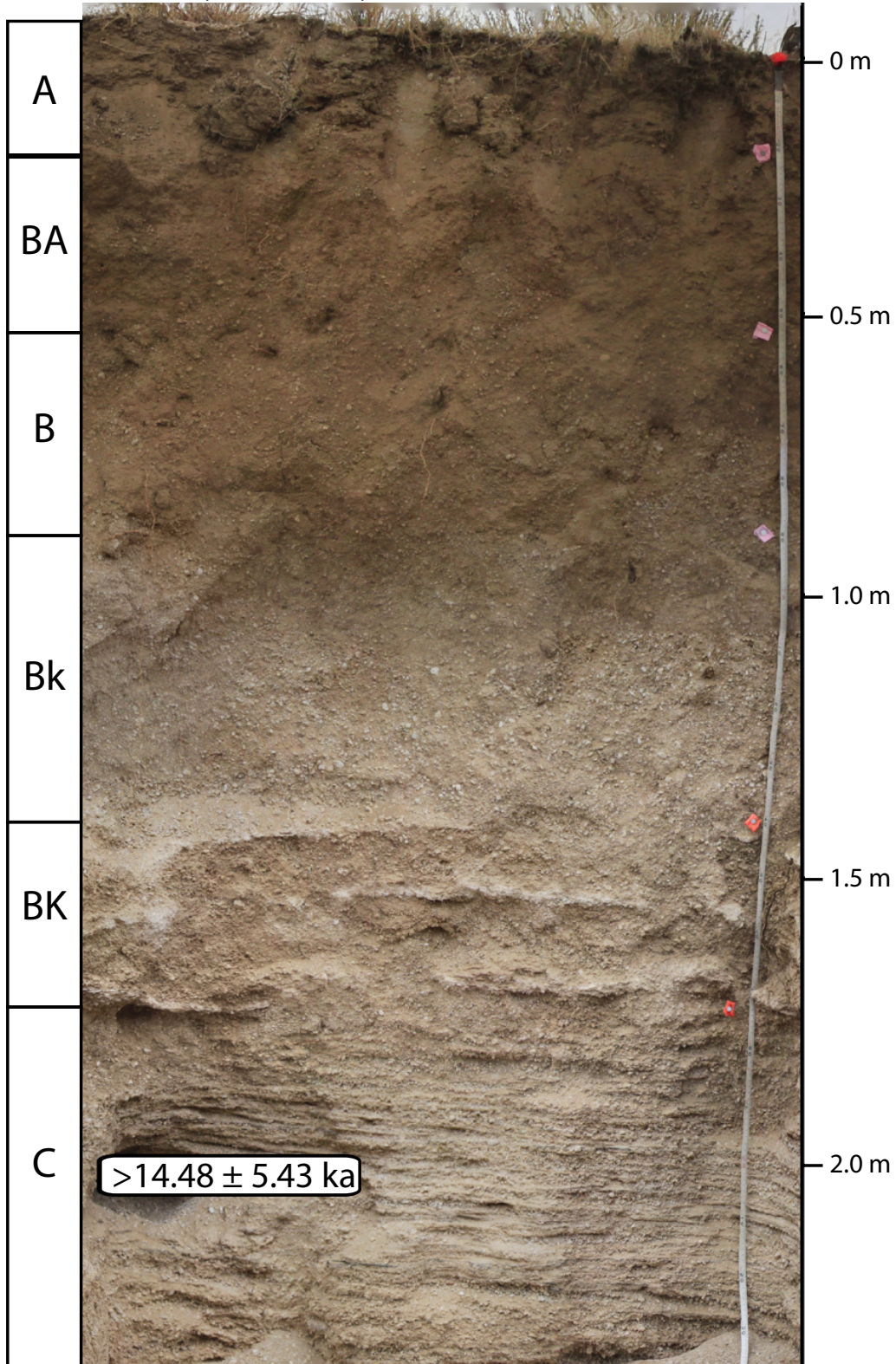
N 38.38123, W 112.90760, 1744 m ASL



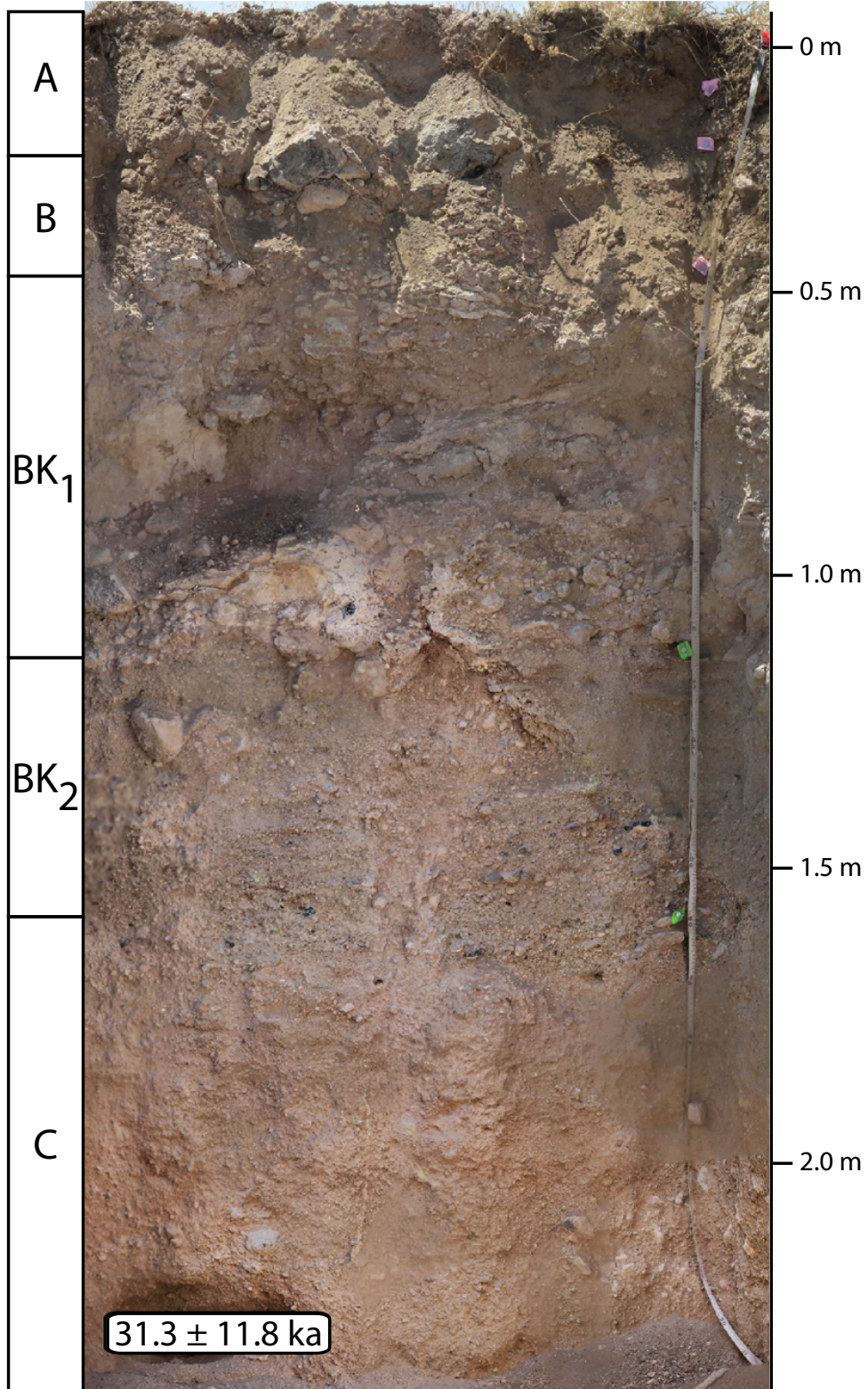
IRSL Site 4b (USU-2684)

Sampled August 24, 2017

N 38.37970, W 112.90788, 1738 m ASL



IRSL Site 5 (USU-2682)
Sampled August 23, 2017
N 38.45210, W 112.86866, 1791 m ASL



Appendix B: Scarp Offset Selection

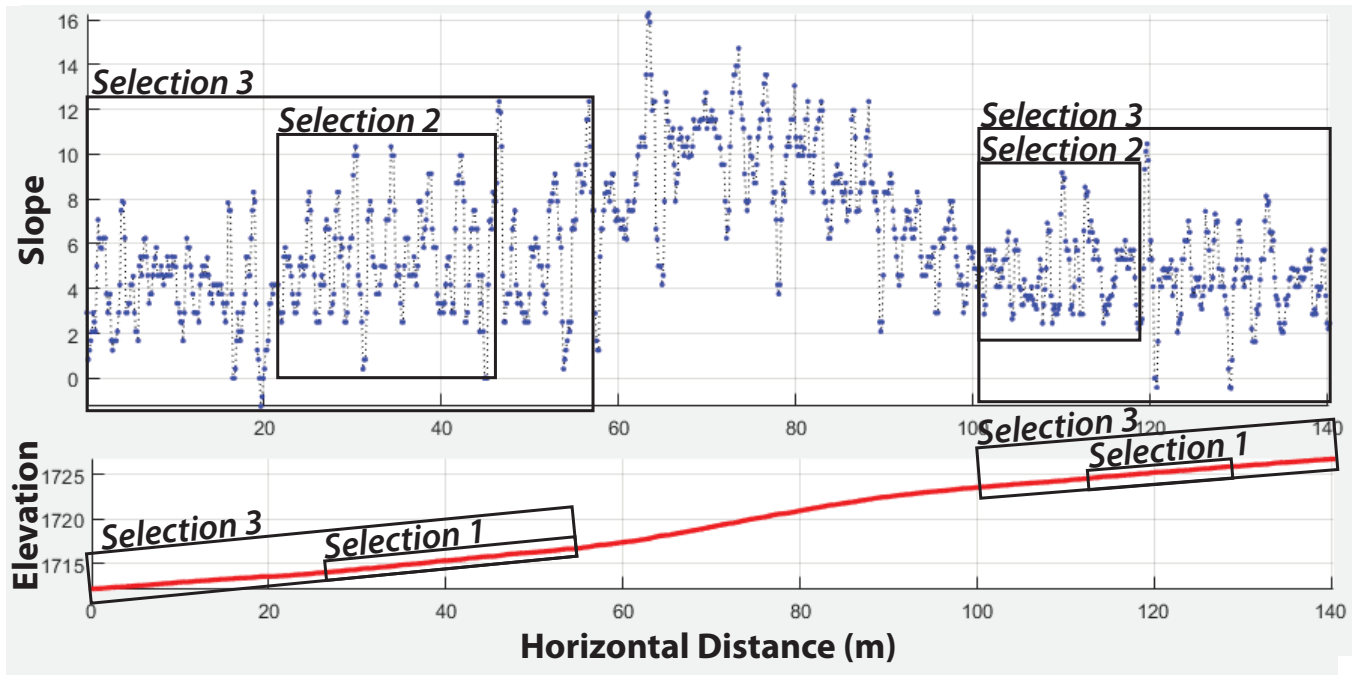


Figure B1. Explanation of methods for selecting the slope defining a fault scarp for geomorphic analysis. The reported fault scarp characteristics are shown in Figure 4 for the OMF and MMWFZ.